



# Plate convergence, foreland development and fault reactivation: primary controls on brine migration, thermal histories and trap breach in the Timor Sea, Australia

Geoffrey W. O'Brien<sup>a,\*</sup>, Mark Lisk<sup>b</sup>, Ian R. Duddy<sup>c</sup>, Joe Hamilton<sup>b</sup>, Phil Woods<sup>d</sup>,  
Robert Cowley<sup>e</sup>

<sup>a</sup>Australian Geological Survey Organisation, G.P.O. Box 378, Canberra, ACT 2601, Australia

<sup>b</sup>CSIRO Petroleum Resources and Australian Petroleum Cooperative Research Centre, P.O. Box 1130, Technology Park, Bentley, WA 6102, Australia

<sup>c</sup>Geotrack International Pty Ltd, 37 Melville Road, Brunswick West, Vic. 3055, Australia

<sup>d</sup>Cultus Petroleum NL, Level 4, 828 Pacific Hwy, Gordon, NSW 2072, Australia

<sup>e</sup>BHP Petroleum, 120 Collins Street, Melbourne, Vic. 3001, Australia

Received 20 January 1998; received in revised form 18 September 1998; accepted 29 September 1998

## Abstract

During the latest Miocene and Early Pliocene (~5.5 MaBP), the collision of the Australian and Eurasian plates resulted in proto-foreland development and significant structural reactivation in the Timor Sea, north-western Australia. Flexural extension, resulting from the down-warping of the Australian plate into the developing Timor Trough, resulted in the dilatation of the major Jurassic and older extensional faults and the formation of shallow Mio-Pliocene fault arrays. An integrated, multidisciplinary study of hydrocarbon traps from this region using 2-D and 3-D seismic data, stable isotope geochemistry, fluid inclusion measurements and apatite fission track data has revealed that this fault reactivation produced three categories of traps: high (HIT), moderate (MIT) and low (LIT) integrity traps. These have characteristic hydrocarbon fill-spill, fluid flow and thermal histories. In MITs and LITs, the dilatation was moderate to intense respectively, and allowed hot (90–130°C), highly saline (200,000+ ppm salinity) brines from deep Palaeozoic evaporites to migrate up the reactivated faults and chemically and thermally affect the reservoir and shallower intervals. Apatite fission track data suggest that fluid migration lasted for between 100,000 and one million years in the case of the MITs, but for only 10,000–100,000 years in the LITs. This major fluid flow event resulted in the development of a prominent, localised Late Tertiary heating ‘spike’ in the MITs, which can significantly affect the accuracy of modelled thermal histories. In the LITs, the thermal effect is less marked, due to the more transient nature of the fluid flow event. HITs were largely unreactivated and hence conduits for brine migration from depth were absent. Consequently, these traps are the most representative of the thermal histories of the source rock depocentres. Where MITs or LITs were charged, the associated loss of fault seal integrity facilitated hydrocarbon loss from the Mesozoic reservoirs, which co-migrated with the brines up through the Mio-Pliocene fault network. Upon entering a shallow, clastic aquifer system (the Eocene Grebe Formation), bacterial oxidation of the hydrocarbons liberated CO<sub>2</sub> which, in turn, resulted in significant and very isotopically light carbonate cementation. This cementation produces sufficient acoustic impedance with the surrounding uncemented sands that it allows these hydrocarbon-related diagenetic zones (HRDZs) to be mapped seismically. Since both the size and acoustic response of the HRDZs are directly proportional to the amount of hydrocarbons that have leaked from the traps, their presence or absence provides a powerful indicator, predrill, of both trap integrity and the likely thermal regime that that traps have experienced. An important observation is that the leaky fault segments over partially breached traps typically only extended for 200–1000 m, whereas over the breached traps, leaky segments extended for 3000–5000 m. Consequently, exploration programs acquiring remote sensing geochemical data (such as geochemical sniffer and airborne laser fluorosensor (ALF) techniques), should have closely spaced line spacings if leaky, potentially commercial fields are to be detected reliably. Potential analogues exist between the processes documented during HRDZ formation, namely the mixing at shallow depths of basinal brines, hydrocarbons and connate waters, and processes occurring during the formation of Pb–Zn and other, low temperature ore deposits. © 1999 Published by Elsevier Science Ltd. All rights reserved.

**Keywords:** Timor Sea; Plate convergence; Foreland development; Mio-Pliocene fault reactivation; Leaky faults; Hydrocarbon-related diagenetic zones (HRDZs); Brine migration; Thermal effects

\* Corresponding author. Tel.: +61-6-249-9342; fax: +61-6-249-9980.

E-mail address: gobrien@agso.gov.au

## 1. Introduction

Poor trap integrity, which relates to Mio-Pliocene collision, foreland development and fault reactivation, is the principal exploration risk in Australia's Timor Sea. In this paper, an innovative, multidisciplinary approach to this problem has been adopted which integrates seismic structural mapping (2-D and 3-D) with detailed, exploration well-based (geochemical and fission track) investigations of the hydrocarbon charge, thermal and fluid flow histories of the assorted trap styles in the region. The goals of this investigation were two-fold: firstly, and principally, to reduce exploration uncertainty associated with trap integrity in the Timor Sea and secondly, to gain a better understanding of the migration of fluids in a modern, developing foreland basin system.

## 2. Geological framework and petroleum habitat

The Timor Sea comprises a system of basin and sub-basin elements which extends from the north-western Australian mainland to the island of Timor (Fig. 1). The region is geologically complex, with individual tectonic elements often having strongly divergent orientations and disparate ages. Localised evaporite deposition in the Siluro-Ordovician was followed by a phase of northeast-southwest oriented crustal extension in the Late Devonian-Early Carboniferous (O'Brien et al., 1993, 1996a). Subsequent rifting episodes in the Early Permian and

Late Jurassic (O'Brien, 1993; O'Brien et al., 1993) took place on an approximate northwest-southeast azimuth, almost orthogonal to the earlier phase. Following continental breakup in the Late Jurassic (Baxter, Cooper, O'Brien, Hill, & Sturrock, 1997), a classic passive margin sequence developed. Early Cretaceous marine shales and mudstones, which provide the principal seal for the Mesozoic petroleum traps in the area, progressively gave way to predominantly shelfal carbonate deposition throughout the Tertiary (Pattillo & Nicholls, 1990).

In the latest Miocene/earliest Pliocene (~5–6 Ma), convergence of the Australian and Eurasian plates established an oblique collisional setting. Uplift of (what is now) the island of Timor and the associated formation of a proto-foreland basin (the Timor Trough; Fig. 1) induced strong flexural stress on the Australian plate inboard from the Timor Trough (O'Brien, Lisk, & Duddy, 1997; O'Brien & Quaife, 1997; O'Brien, Quaife, & Messent, 1998a; O'Brien et al., 1998b). The associated extensional fault reactivation of the deeper Palaeozoic and Mesozoic fault arrays produced Mio-Pliocene-aged faults, with displacements ranging from subseismic (<20–30 m) to greater than 300 m, which have led to the partial or complete breach of the top and/or fault seal in many previously charged traps (O'Brien & Woods, 1995a, 1995b; O'Brien et al., 1996b, 1997, 1998a, 1998b; O'Brien & Quaife, 1997).

At approximately 2.5 Ma, the regional stress regime changed significantly: volcanism and thrusting on Timor island stopped and convergence of Timor and the Australian mainland appears to have ceased (Abbott & Chamalaun, 1981; McCaffrey, 1988; Genrich et al., 1995). The throws on the flexural faults within the Timor Sea reflect this change in regional stress: from about 2.5 Ma, throws on the flexural faults decreased dramatically (O'Brien & Quaife, 1997; O'Brien et al., 1998a, 1998b).

The petroleum exploration history of the region mirrors this geological complexity. The region is highly prospective, as evidenced by the numerous oil and gas condensate discoveries in and around the Sahul Platform and Sahul Syncline (e.g. Elang, Bayu-Undan, Laminaria, Buffalo) and the Vulcan Sub-basin (Skua, Jabiru, Challis, Tenacious). These traps are all fault-bounded horsts that formed in the Late Jurassic (Pattillo & Nicholls, 1990) and consist of combinations of Mesozoic reservoirs (principally Triassic and Early-Middle Jurassic sands), with Late Jurassic or (more typically) Early Cretaceous top seals. The source rocks are almost exclusively considered to comprise Late Jurassic shales of the Lower Vulcan Formation (Fig. 2).

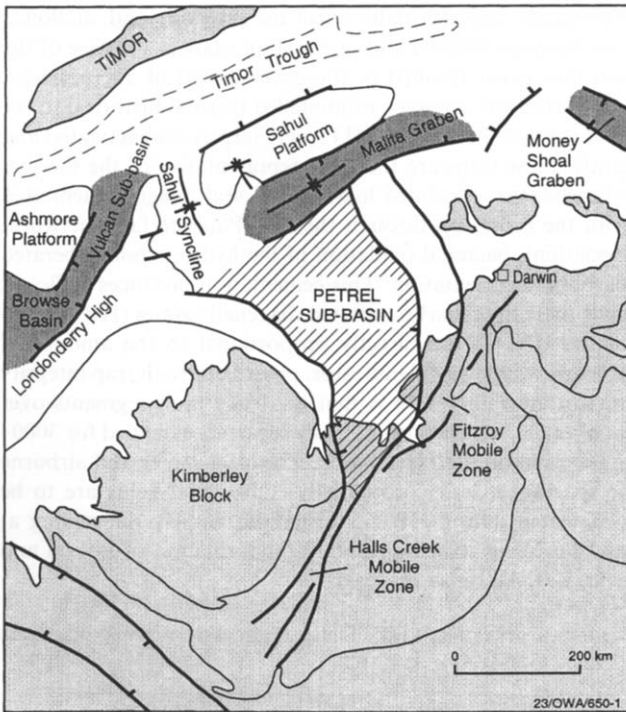


Fig. 1. Location map showing the tectonic elements of the Timor Sea, north-western Australia.

## 3. Study rationale and focus

In spite of the area's demonstrated petroleum prospectivity, the issue of poor trap integrity has proven to

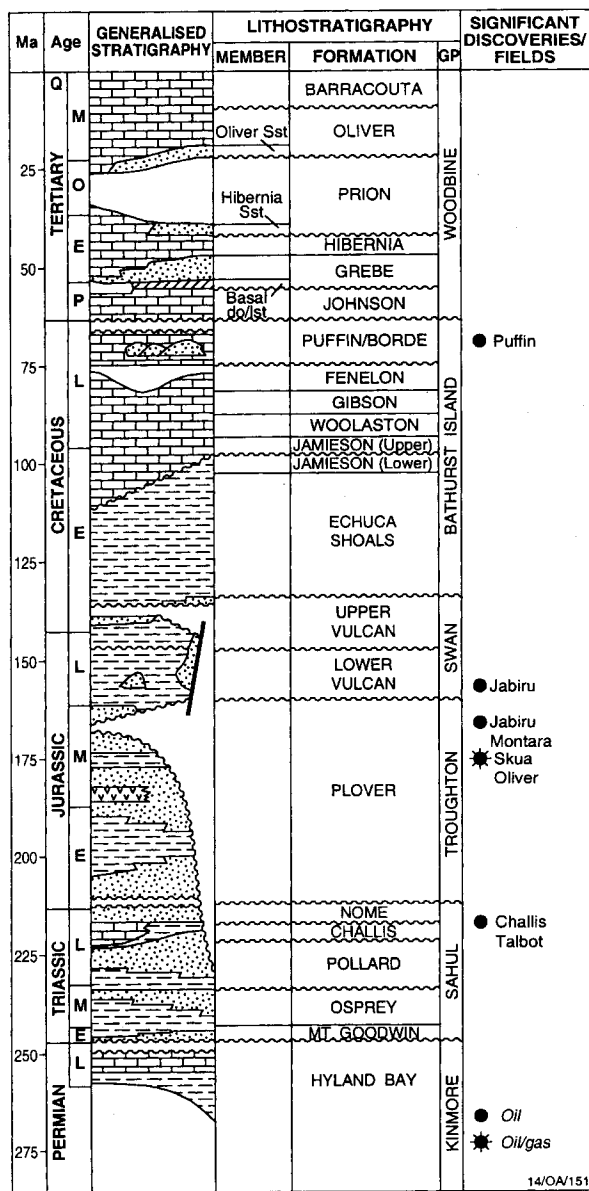


Fig. 2. Stratigraphic column for the Vulcan Sub-basin. Modified from Osborne (1990).

be a major (indeed the major) uncertainty in exploring within this region. Given the large numbers of residual oil columns that have been drilled (e.g. Swift, East Swan, Eclipse, Avocet; Fig. 3), any improvement in the ability to evaluate trap integrity, predrill, would have a significant effect in maximising the effectiveness of exploration dollars spent.

To this end, part of the Australian Geological Survey Organisation's (AGSO) ongoing regional research program within the Timor Sea has been focussed on obtaining a better understanding of both trap integrity and fluid flow. This multiinstitutional, multidisciplinary research program (the Fill–Spill Project) has been designed to provide the exploration industry with a regional to semi-

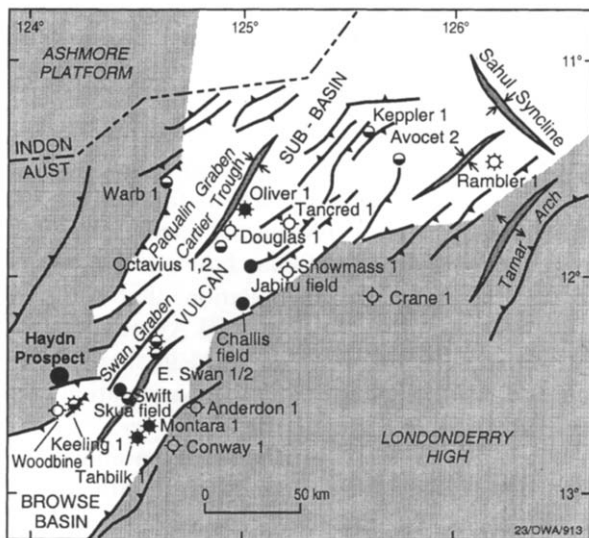


Fig. 3. Location map of the Vulcan Sub-basin, showing key structural elements and exploration wells. Highlighted wells were investigated during the present study.

regional interpretative framework within which to interpret trap integrity and fluid flow at a prospect-scale. To date, several integrated remote sensing acquisition programs have been carried out over key areas within the Timor Sea; acquisition programs have included high-resolution aeromagnetic data, 2-D seismic data, high resolution water bottom geochemical ‘sniffer’ (500 m line spacing) data and airborne laser fluorosensor (ALF) acquisition (300 m line spacing) data.

In this paper, we present the results of the integration of 2-D seismic and sniffer data acquired during one of these programs within the Vulcan Sub-basin (Figs. 1 and 3) with analytical data derived from exploration well-based studies of the reservoir and overlying sequences from the same area. Analyses included stable isotopic (carbon, oxygen, strontium) to characterise the nature and origin of migrating fluids, fluid inclusion measurements to determine palaeo-oil saturation, as well as microthermometry and palaeo-salinity measurements to characterise migrating fluids andapatite fission track analysis (AFTA<sup>®</sup>) to determine thermal histories.

This paper expands upon recent work which has addressed the issue of trap integrity in the Timor Sea (O'Brien & Woods, 1994, 1995a, 1995b; O'Brien et al., 1996b, 1997; O'Brien, Woods, Lisk, Fellows, & AGSO, 1996c; O'Brien & Quaife, 1997).

#### 4. Trap integrity investigations in the Timor Sea

##### 4.1. Hydrocarbon-related diagenetic zones (HRDZs): the ‘fingerprint’ of leaky traps

A key result of previous investigations into trap integrity in the Timor Sea (O'Brien & Woods, 1994, 1995a,

1995b; O'Brien et al., 1996b, 1996c) was the recognition of the significance of localised, strongly carbonate-cemented zones within shallow marine sands of the Eocene Grebe Formation (Fig. 2). These cemented zones are variable in size (<100–5000 m) and typically occur closely associated with Mio-Pliocene fault arrays overlying charged or breached Mesozoic traps. For example, they are present over the Skua, Jabiru and Challis oil fields, and the breached accumulations that were tested by the Swift, East Swan, Eclipse and Avocet wells (Fig. 3). The zones are lenticular to ovoid in shape and are oriented ENE to NE, parallel to the orientation of the Mio-Pliocene faults.

The localised, intense carbonate cementation results in a strong acoustic impedance contrast with adjacent, uncemented Eocene sands, and, as a consequence, the cemented zones can be imaged clearly on seismic data (Fig. 4a and b). The cementation induces significant seismic velocity ‘pull-up’, thereby producing apparent time ‘highs’ at the underlying Top Paleocene interval, as well as a loss of stack response integrity and data quality below the cemented zones. These effects can be used to map the carbonate cemented zones, particularly using 3-D seismic data sets.

In the Vulcan Sub-basin, the close spatial association of carbonate cemented sandstones with partially and completely breached accumulations indicates that the relationship between the cementation and hydrocarbon seepage may be causal, given that surface and near-surface carbonate cementation in the US Gulf Coast, the Irish Sea and the North Sea is commonly associated with the bacterial oxidation of migrating hydrocarbons (Hovland, Talbot, Qvale, Olaussen, & Aasberg, 1987; Roberts, Sassen, & Aharon, 1987; Aharon, Roberts, Sassen, Wheeler, & Feng, 1989; Roberts, Sassen, Carney, & Aharon, 1989a; 1989b; Roberts, Sassen, Carney, Aharon, & Portier, 1989c; Roberts, Aharon, Carney, Larkin, & Sassen, 1990; Aharon, Roberts, Sassen, & Larkin, 1990; Brooks et al., 1990; Roberts, Aharon, & Mueller, 1991; Sassen, Grayson, Cole, Roberts, & Aharon, 1991a; 1991b; Aharon, Gruber, & Roberts, 1991a; 1991b; 1992a; Aharon, Roberts, & Snelling, 1992b; Anderson, Aharon, & Gupta, 1992; Gruber, Aharon, & Roberts, 1990; Sassen et al., 1993; Hovland, Croker, & Martin, 1994). Clearly, if this relationship in the Timor Sea is causal, then the presence or absence of cemented zones over individual structures could provide information on whether the structure has been charged and whether on it has maintained its fault seal integrity during reactivation.

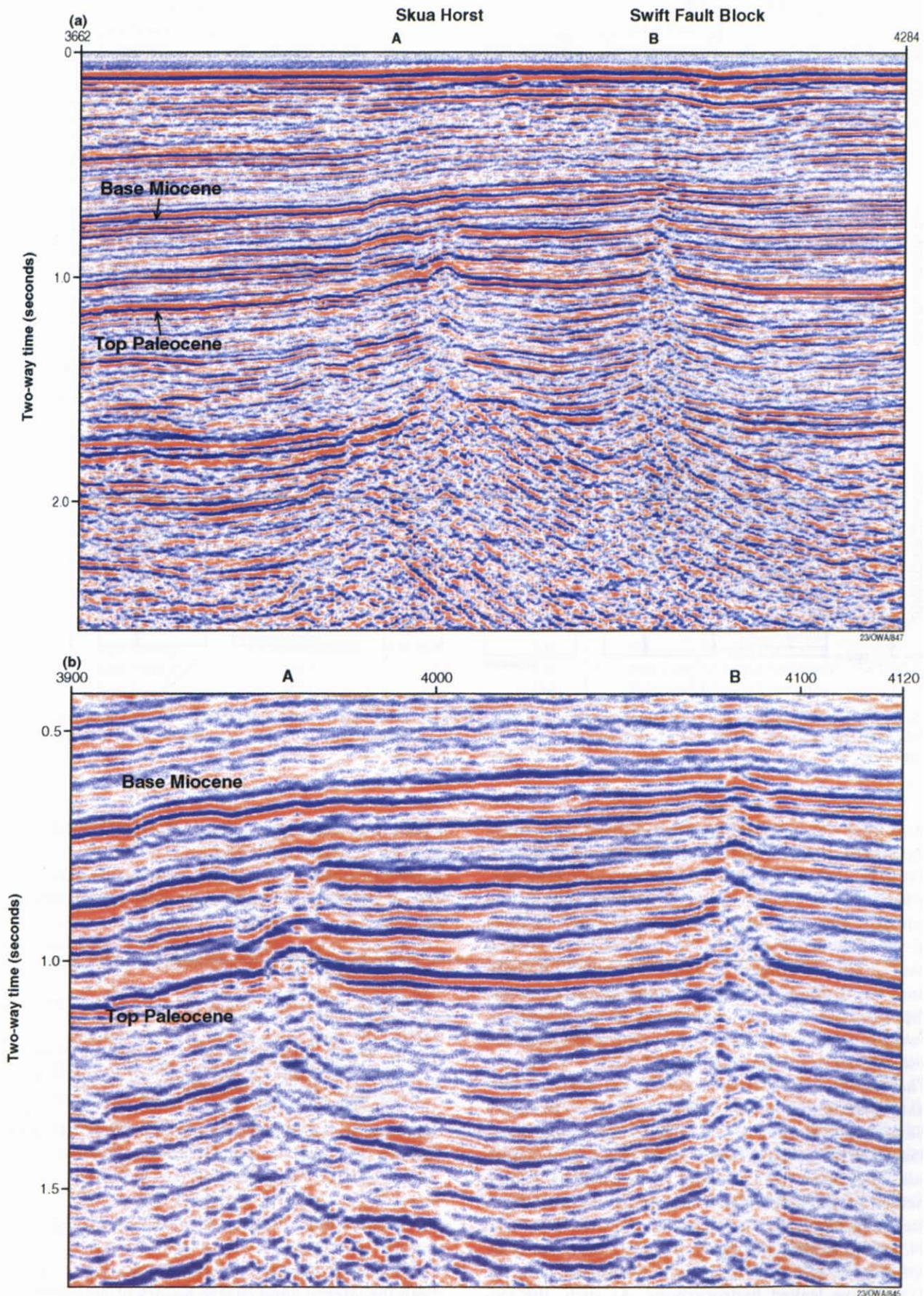
To determine the nature of the relationship, a systematic petrographic and stable isotopic investigation of several traps that had actually drilled through a cemented zone was carried out (O'Brien & Woods, 1995a, 1995b; O'Brien et al., 1996b). Wells investigated included Skua 3, Jabiru 2, East Swan 2 and Keeling 1. The cemented Grebe Formation sands within all of these wells are fairly similar petrographically and consist of fine to very coarse grained, angular to well-rounded quartz with a pervasive carbonate cement. The dominant cement is a poikilotopic, low magnesium calcite; poikilotopic dolomite/ankerite spar is generally subordinate (an exception was Skua 3), with rhombs occasionally present. Both the dolomite spar and the rhombs appear to post-date the calcite.

In order to determine whether the carbonate cements within the Eocene Grebe Formation were indeed hydrocarbon-related, carbon and oxygen isotope analyses were run through the interval in the East Swan 2 well (Fig. 5a; Table 1). The East Swan structure comprises a breached accumulation with a large and seismically intense cemented zone developed within the Grebe sands (Fig. 6). An interpretative framework for these results was provided by a similar analytical series run through the same interval in the East Swan 1 well, which was located approximately 1400 m south of the East Swan 2 well, just outside the seismically-defined zone of cementation (Fig. 6b).

The results of this investigation are shown in Fig. 5a and b and Table 1. The sonic log for the East Swan 2 well (Fig. 5b) shows that the Grebe sand is uniformly fast, due to pervasive carbonate cementation, with average transit velocities of ~180  $\mu\text{s}/\text{m}$  and very light carbon isotope values (to  $\sim -25 \delta^{13}\text{C}$ ). The light  $\delta^{13}\text{C}$  values within the cemented Grebe Formation sands are consistent with those of carbonate cements which have formed principally via the bacterial oxidation of migrating hydrocarbons. The values are generally similar to those of carbonates associated with areas of active hydrocarbon seepage in the US Gulf Coast (Roberts et al., 1987, 1989a, 1989b, 1989c, 1990, 1991; Aharon et al., 1989, 1990, 1991a, 1991b, 1992a, 1992b; Anderson et al., 1992; Sassen et al., 1991, 1993).

Compare the profile through East Swan 2 (Fig. 5b) with an identical profile through the East Swan 1 well (Fig. 5a), which was drilled outside the seismically-defined zone of cementation (Fig. 6a). The sonic velocities in East Swan 1 average  $\sim 350 \mu\text{secs}/\text{m}$ , approximately half those in East Swan 2, confirming their weakly cemented nature. Similarly, the carbon isotopic values in

Fig. 4. (a) Regional seismic section (AGSO 98R/8) showing carbonate cemented, hydrocarbon-related diagenetic zones (HRDZs) over the Skua ('A') and Swift ('B') fields. The HRDZ associated with the commercial Skua Field ('A') is about 0.5 by 1 km, whereas the HRDZ over breached Swift accumulation is much larger (1  $\times$  4 km). (b) Detailed view of Fig. 4a.



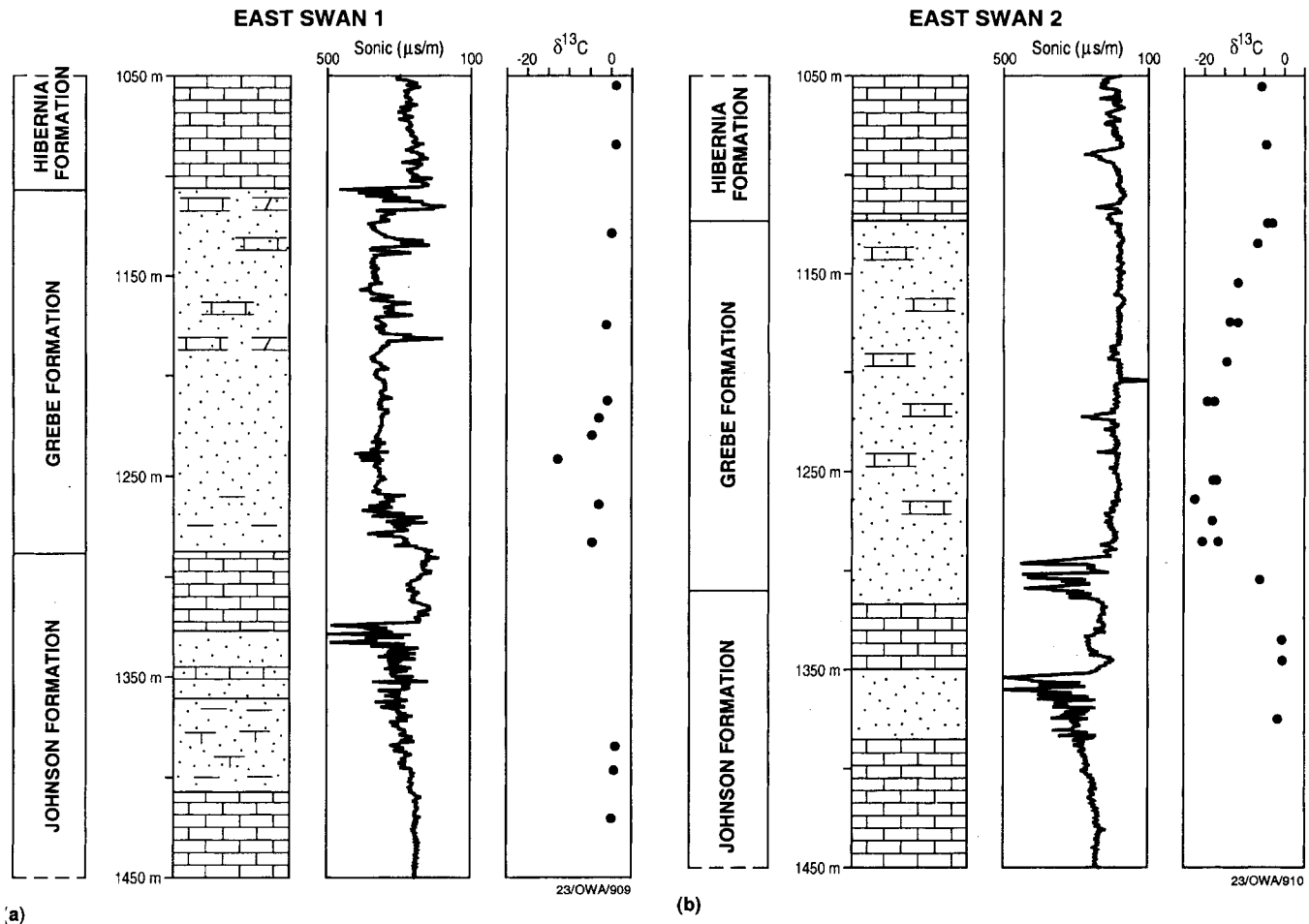


Fig. 5. (a) Tertiary section in East Swan-1, showing velocity information in relation to carbon isotopic composition of carbonates and carbonate cements. (b) Tertiary section in East Swan-2, showing velocity information in relation to carbon isotopic composition of carbonates and carbonate cements.

East Swan 1 are typical of syn-depositional/early diagenetic marine cements, and are significantly heavier (usually 0 to  $-3$ ) than those in East Swan 2. Nevertheless, one light carbon isotopic value (Fig. 5a; Table 1) was obtained at 1241 m ( $-12.5$ ) in East Swan 1. This suggests that a geochemically resolvable 'halo zone' of weak cementation/hydrocarbon oxidation extends beyond the boundaries of the seismically-resolvable cemented areas; in the halo zone, acoustic impedance differences between the weakly cemented and uncemented sands are probably too small to allow seismic definition.

The stable isotopic data thus confirm that the carbonate cementation at East Swan 2 (as well as in Jabiru 2, Skua 3 and Keeling 1; see O'Brien & Woods, 1994, 1995a; O'Brien et al., 1996b, 1996c) is related to diagenesis associated with leaking hydrocarbons. These cemented zones, which have been termed 'hydrocarbon-related diagenetic zones' or 'HRDZs' (O'Brien & Woods, 1994, 1995a, 1995b; O'Brien et al., 1996b, 1996c) provide proof that the Mesozoic traps or fault systems below the HRDZs have leaked hydrocarbons. As such, the rec-

ognition of the significance of the HRDZs has proven critical.

The presence of an HRDZ, or several HRDZs, over a trap provides several pieces of information about the structure. These include

- HRDZs indicate that *the trap was charged prior to reactivation*.
- HRDZs indicate that *the trap has leaked after reactivation*.
- The size of individual HRDZs could provide *direct information about the total length of the fault segments which have leaked within respective structures*.

Conversely, the absence of HRDZs over a trap might indicate that the structure was *never charged* or, alternatively, that it has *never leaked*.

#### 4.2. Relationship between structural style and trap integrity

Given that HRDZs can provide unique insights into both the integrity and charge history of petroleum traps,

Table 1  
Stable isotopic measurements for the East Swan-1 and -2 wells in the Timor Sea

Well	Depth (m)	$\delta^{13}\text{C}$	$\delta^{18}\text{O}$	Formation/age
East Swan-1	1001	1.2	-3.41	Eocene Hibernia Formation
East Swan-1	1056	1.34	-4.05	Eocene Hibernia Formation
East Swan-1	1084	1.34	-3.56	Eocene Hibernia Formation
East Swan-1	1129	0.06	-0.37	Grebe Formation, Eocene
East Swan-1	1175	-0.93	-2.18	Grebe Formation, Eocene
East Swan-1	1212	-0.54	-2.56	Grebe Formation, Eocene
East Swan-1	1221	-3.04	-3.61	Grebe Formation, Eocene
East Swan-1	1230	-4.86	-5.00	Grebe Formation, Eocene
East Swan-1	1241	-12.48	-6.76	Grebe Formation, Eocene
East Swan-1	1266	-3.44	-2.12	Grebe Formation, Eocene
East Swan-1	1282	-4.36	-2.08	Grebe Formation, Eocene
East Swan-1	1385	1.66	-2.68	Paleocene Johnson Formation
East Swan-1	1398	1.43	-2.63	Paleocene Johnson Formation
East Swan-1	1425	0.37	-2.74	Paleocene Johnson Formation
East Swan-1	1574	3.9	-3.26	Paleocene Johnson Formation
East Swan 2	1005	-2.32	-3.99	Eocene Hibernia Formation
East Swan 2	1055	-5.58	-4.57	Eocene Hibernia Formation
East Swan 2	1085	-4.78	-4.80	Eocene Hibernia Formation
East Swan 2	1125	-4.12	-4.84	Eocene Hibernia Formation
East Swan 2	1155	-11.51	-3.79	Grebe Formation, Eocene
East Swan 2	1175	-11.40	-5.10	Grebe Formation, Eocene
East Swan 2	1195	-14.41	-4.31	Grebe Formation, Eocene
East Swan 2	1215	-17.30	-5.40	Grebe Formation, Eocene
East Swan 2	1255	-17.80	-5.50	Grebe Formation, Eocene
East Swan 2	1265	-22.72	-5.63	Grebe Formation, Eocene
East Swan 2	1285	-20.30	-5.80	Grebe Formation, Eocene
East Swan 2	1335	-0.88	-2.98	Paleocene Johnson Formation
East Swan 2	1345	-0.55	-2.93	Paleocene Johnson Formation
East Swan 2	1375	1.57	-3.01	Paleocene Johnson Formation
East Swan 2	1455	2.67	-3.34	Paleocene Johnson Formation
East Swan 2	1575	3.02	-3.84	Paleocene Johnson Formation

and given that HRDZs can be mapped reliably using seismic data, a systematic, seismically-based structural investigation was carried out over a range of trap types within the Timor Sea. The principal emphasis of this study was to investigate the relationship between the structural style of individual traps (particularly in relation to the association between the Jurassic (rift) and Mio-Pliocene (reactivation) faults) and the size and distribution of the HRDZs over the respective traps.

Trap/accumulation types investigated (Fig. 3) included subcommercial gas accumulations (e.g. the Oliver and Montara fields), oil accumulations (including the producing Jabiru and Skua fields), and breached accumulations (e.g. the East Swan, Swift and Avocet structures).

#### 4.2.1. Gas accumulations

The gas accumulations within the Vulcan Sub-basin are typically filled to ‘spill’ and contain thin associated oil legs. They fall into two structural categories. The first, of which the Montara field is representative, shows little or no Mio-Pliocene fault reactivation. Such traps are

generally located in ‘intrabasinal’ settings, over Jurassic rift faults of only moderate ( $< \sim 500$  m) displacement. The second category, represented by the Oliver field, shows very significant (up to 300–350 m) Mio-Pliocene fault displacement over moderate displacement Jurassic faults. The Mio-Pliocene faulting at Oliver is precisely aligned (divergences are  $< 5^\circ$ ) with, and actually links directly into, the deeper, Mesozoic rift faults.

Both styles of gas accumulation have no attendant HRDZs and hence have leaked very little, if at all. This has been confirmed by recent fluid inclusion studies (O’Brien et al., 1996b; Lisk, O’Brien, & Brincat, 1997) which have shown that traps such as Montara and Oliver have characteristically contained an earlier oil charge which was subsequently partially displaced by gas migrating into the traps in the Late Tertiary (Gussow displacement). Further confirmation for a distinct lack of seepage over this trap type comes from recent geochemical ‘sniffer’ and airborne laser fluorescence studies (O’Brien & Woods, 1995a, 1995b; O’Brien et al., 1998a, 1998b).

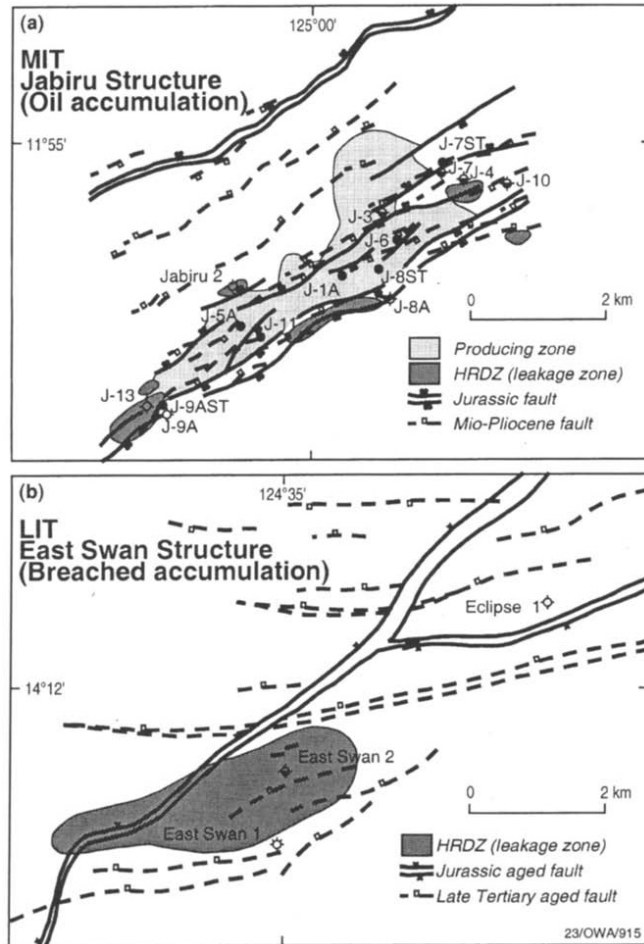


Fig. 6. Comparison between the seismically-mapped Jurassic and Late Tertiary fault trends and the distribution of the HRDZs over the Jabiru (a) and East Swan (b) structures. Modified from O'Brien and Woods (1995a).

Given the lack of leakage over these traps, accumulations such as Montara and Oliver clearly have a *high (fault and top) sealing capacity for both oil and gas*.

#### 4.2.2. Oil accumulations

Major oil fields within the Vulcan Sub-basin, such as those at Skua, Jabiru and Challis, show generally similar structural, reactivation and seepage styles. All are located on large displacement (> 500 m to ~ 1500 m), NE-trending Callovian-aged rift faults; Mio-Pliocene reactivation faults range from ~ 50 m at Skua, with a divergence from the underpinning Callovian faults of about 20–25°, to about 150–180 m at Jabiru, with a divergence of approximately 5°. The Mio-Pliocene fault arrays which develop over these traps are generally quite narrow (~ 2–3 km wide), with their location tightly determined by the underpinning Jurassic rift fault.

Fluid inclusion data (O'Brien et al., 1996b) confirm that all of the major oil accumulations within the Vulcan Sub-basin, including the Skua, Jabiru and Challis fields, have small to significant basal residual oil columns and

have experienced minor to significant leakage. These fields have associated lenticular- to ovoid-shaped HRDZs, which are small- to moderate-sized (usually in the range 200–1000 m long, occasionally 1500 m long), and are distributed around the periphery of the palaeo- and present day accumulations. For example, at Jabiru (Fig. 6a), the HRDZs are located outside the present day accumulation, suggesting that they formed initially when the field was larger than it is today. As such, the HRDZs actually reflect the 'pre-reactivation/leakage' geometries of the traps. The HRDZs are typically controlled spatially by the Mio-Pliocene fault arrays, and are relatively narrow, with a width of 200 m, to a maximum of 500 m.

Minor leakage from these traps is continuing today, as evidenced by low level hydrocarbon seepage detected via sniffer and ALF from faults bounding the Skua and Jabiru accumulations (O'Brien & Woods, 1995a, 1995b; O'Brien et al., 1998a, 1998b).

Neither the Skua, Jabiru or Challis fields contain gas caps within fault-controlled closure (O'Brien & Woods, 1995a, 1995b) and are presently undersaturated with respect to gas (O'Brien et al., 1996b). This is in spite of the fact that the source kitchens which have charged these traps are presently generating and expelling large amounts of gas (O'Brien et al., 1998b). These observations, when combined with the fact that these traps are leaking (albeit at low levels) at the present day, suggest that *these traps have moderate fault sealing capacity for oil, but only low sealing capacity for gas*. This combination has effectively allowed the amount of gas entering the structures to be largely matched by gas progressively 'bleeding' off up the Mio-Pliocene fault systems.

#### 4.2.3. Breached accumulations

As with the gas- and oil-bearing traps, the breached traps show characteristic structural and reactivation styles. These traps are generally located on very large displacement (> 1500 m) Jurassic rift faults, over which has developed a strongly oblique (divergence 30–50°) and quite broad (5–6 km wide) Mio-Pliocene fault array which itself has displacements in the range 250–350 m. The Mio-Pliocene faults are effectively Riedel shears above the underpinning rift faults, and it is likely that, at least in some instances, they have helicoidal geometries, similar to those described by Richard, Naylor and Koopman (1995) in analogue modelling experiments.

Fluid inclusion investigations (O'Brien et al., 1996b) using the GOI technique (percentage of grains with oil inclusions) have established that traps such as East Swan and Eclipse both originally contained oil columns approximately 100 m thick, implying the loss of massive (estimated > 100 million barrels) amounts of oil. This is consistent with the large and seismically-intense nature of the HRDZs which have been mapped above such traps. For example, at East Swan (Fig. 6b), the HRDZ is approximately 1 × 5 km in size and is aligned precisely

with a major Mio-Pliocene fault, which trends at a very high angle to the deeper rift fault. Lengths of 3–5 km and widths of 0.5 to 1 km, appear typical for HRDZs located above breached traps.

Remote sensing geochemical techniques, such as geochemical sniffer and ALF, have demonstrated that these breached traps display only very low levels of present day seepage. This seepage probably represents the present day hydrocarbon charge which is migrating into the Mesozoic reservoirs within these traps and is then continuously leaking upwards to the seafloor (O'Brien et al., 1998a, 1998b).

#### 4.2.4. Summary of key observations

The observations presented above are summarised schematically in Fig. 7a–d. In the Early Miocene, charged traps in the region were all of high integrity, with a high sealing capacity for oil and gas; the traps may or may not have had a gas cap. At approximately 5.5 MaBP, convergence of the Australian and Eurasian Plates, and proto-foreland development in the Timor Trough, induced significant, flexurally-driven fault reactivation.

In some traps, fault reactivation was minimal, or at least had a minimal effect, and the integrity of the traps was maintained (Fig. 7b). Key factors in maintaining trap integrity appear to involve combinations of

- Relatively small displacements on the deeper Jurassic faults, which favoured minimal reactivation. The resulting Neogene faults were of either small displacement, or did not develop at all.
- Where Mio-Pliocene faults have larger displacements (as at Oliver), the coalignment ( $<5^\circ$ ) of the Jurassic and Mio-Pliocene fault arrays is important.

In this ‘high integrity’ structural scenario, progressive maturation of the source rocks, when combined with a lack of leakage from the traps, led to the progressive flushing of the oil accumulation with gas in the Late Tertiary (Fig. 7b). This flushing, given the relatively small trap sizes in the region, led to the formation of a sub-commercial gas, or subcommercial mixed gas–oil, accumulations.

Where reactivation was moderate, a relatively narrow Mio-Pliocene fault array developed directly over the underpinning rift fault (Fig. 7c). These Mio-Pliocene faults were closely aligned to the deeper faults ( $>5$  to  $<\sim 25^\circ$ ), and had small to moderate displacements. Fault reactivation decreased seal integrity, which facilitated the loss of all of the gas and some of the oil from the Mesozoic reservoir units. The lost hydrocarbons migrated vertically until they reached the Eocene Grebe Formation sands, which were acting as a basin-wide aquifer at relatively shallow depth ( $\sim 500$  m at 5.5 MaBP). Biodegradation of the migrating hydrocarbons liberated CO<sub>2</sub> for incorporation into calcite or dolomite cements, thereby producing (isotopically light) HRDZs. The

decreased fault seal integrity reduces the likelihood of gas flushing for this style of trap, as gas migrating into the trap in the Late Tertiary simply ‘bleeds’ directly up the fault.

The distribution of the HRDZs shows that over producing oil accumulations (i.e. accumulations that have *maintained commercially viable volumes of hydrocarbons*), the leaky fault segments usually extend for only a few hundred metres (occasionally up to 1500 m) and that the faults do not leak along their entire length. This is an important observation, since it proves that hydrocarbons debouching onto the seafloor over a leaky commercial trap in the Timor Sea would do so at ‘point sources’, which would be very difficult to detect using remote sensing data acquired on a wide (3 km, for example) grid.

Breached traps are typically located over very large displacement Jurassic rift faults, which appear to have favoured the development of attendant large displacement Mio-Pliocene fault arrays (Fig. 7d). A broad zone or cone of Mio-Pliocene fault ‘damage’ typically radiates from the deeper rift faults, with a generally very strong ( $>30\text{--}50^\circ$ ) obliquity present between the two fault sets. Total failure of fault seal produced a massive flux of hydrocarbons through the Tertiary, with massive cementation developing within the Grebe Formation sands. Faults over breached traps have leaked for between 3 and 5 km along their length and have produced a zone of HRDZ formation 1 km wide.

It appears that a critical Mio-Pliocene gross fault displacement exists for retaining fault seal integrity. This appears to be about 200–250 m across the trap; beyond this displacement, traps are invariably breached where any obliquity exists between the rift and reactivation faults. It may be that this observation relates to the total thickness of the regional seal in this area, the Early Cretaceous Echuca Shoals Formation. Similarly, the obliquity between the Mio-Pliocene fault arrays and the Jurassic faults may be important simply because an oblique geometry, coupled with large Mio-Pliocene fault displacements, would favour in seal breach in the middle of the trap, near the top of structural closure, thereby ensuring complete loss of the accumulation. In contrast, where the respective fault sets are more parallel, leakage tends to occur around the periphery of the trap, resulting in only partial loss of column.

Integration of observations on the size of the developed HRDZs with the geometric relationship between the Jurassic and Mio-Pliocene fault sets have provided a predictive capability for evaluating the likely integrity, and charge history, of undrilled traps in the Timor Sea (Fig. 8).

#### 4.3. Tripartite trap classification

The previous discussion on the structural characteristics of the gas, oil and breached accumulations in the

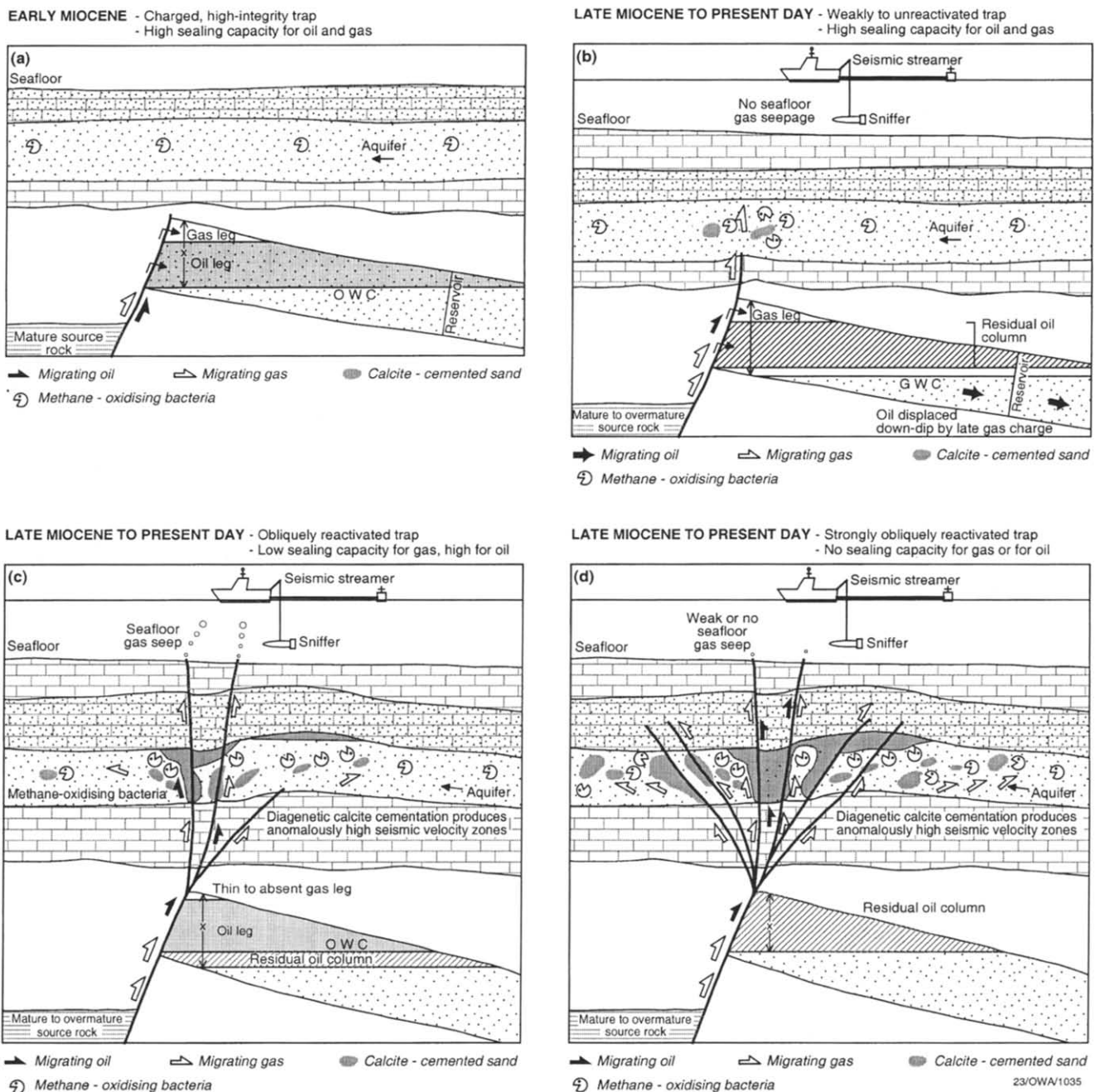


Fig. 7. Schematics which document the progressive reactivation of a high integrity, oil and gas accumulation (a; pictured at Early Miocene time) which results from the collision of the Australian and Eurasian plates in the Late Miocene/Early Pliocene. A continuum exists between unreactivated traps which are prone to gas-flushing (b), to moderately reactivated traps which are typically commercial oil accumulations (c) to very strongly reactivated and breached accumulations (d). Hydrocarbons leaking up the faults are oxidised by methane-oxidising/sulphate-reducing bacteria within the Grebe Formation aquifer. The released CO<sub>2</sub> is incorporated into pervasive carbonate cementation along the fault zone.

Timor Sea highlights the fact that a broad tripartite trap classification, based upon trap integrity, is possible. This classification consists of

- High integrity traps (HITs): have a high seal integrity with respect to both oil and gas and are now often

partially to completely gas-flushed. Examples include the Oliver and Montara traps.

- Moderate integrity traps (MITs): have a moderate seal integrity with respect to oil, but a relatively low sealing capacity with respect to gas. Examples include the Skua, Jabiru and Challis producing oil fields.

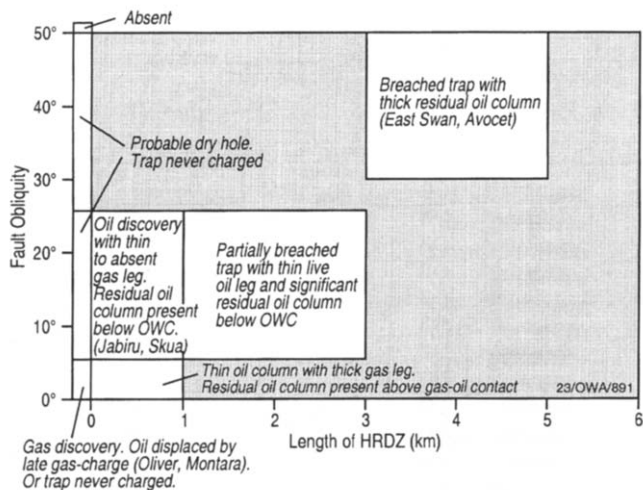


Fig. 8. Simplistic representation of the relationships between the nature of Mio-Pliocene fault reactivation and the size of hydrocarbon-related diagenetic zones (HRDZs) in the Vulcan Sub-basin, Timor Sea. Figure constructed from information in Tables 3 and 4 of O'Brien and Woods (1995a).

- Low integrity traps (LITs): have a poor sealing capacity for both oil and gas and have been completely breached. Examples include the East Swan, Eclipse and Avocet breached accumulations.

## 5. Relationship of fluid flow and thermal histories to trap integrity

In this section, the fluid flow and thermal histories of representative traps within the tripartite classification have been characterised. Specifically, an attempt has been made to elucidate the role that basinal, saline brines may have played during HRDZ formation over MITs and LITs. For example, O'Brien and Woods (1995a; 1995b) proposed (citing the fluid inclusion data of Eadington & Hamilton, 1990), that very saline, high temperature brines were migrating during HRDZ formation and may have provided the cations and anions for the formation of the calcite and dolomite cements which comprise the HRDZs. Similarly, given the apparent high salinities (>200,000 ppm) and temperatures (>100 °C) of these brines (Eadington & Hamilton, 1990), significant, though quite localised, Late Tertiary diagenetic and thermal/maturation effects could be produced by their passage.

During our investigation, a large number of traps were investigated. Palaeo-thermometry and palaeo-salinity data were either already available (Eadington, Lisk, & Hamilton, 1990; Eadington & Hamilton, 1990; Lisk, Hamilton, & Eadington, 1992), or were acquired, for the following wells.

HITs: Oliver-1.

MITs: Jabiru-1A and -2, Challis-1, Skua-3, Douglas-1, Octavius-1 and -2.

LITs: East Swan-2.

Palaeo-thermometry and palaeo-salinity data were obtained throughout the Mesozoic reservoir units in all wells; data were also acquired from the Eocene Grebe Formation, the site of HRDZ formation, in Jabiru-1A and -2 and East Swan-2.

Apatite fission track analysis (AFTA<sup>R</sup>) data for assorted wells in the Timor Sea were assembled from open-file reports (Geotrack, 1987, 1988, 1997) and were supplemented by additional sampling and analysis (O'Brien et al., 1996b; Geotrack, 1997). The following wells were analysed via AFTA<sup>R</sup>.

HITs: Oliver-1; Montara-1.

MITs: Challis-1 and 5; Jabiru 1A and 2; Tancred-1; Snowmass-1; Douglas-1.

LITs: East Swan-1 and 2.

For the purposes of brevity, the following traps, which are representative of their respective trap types, will be discussed in detail in terms of both their fluid flow and thermal histories. These wells are Oliver-1 (HIT), Challis-1 and -5 and Jabiru-1A and -2 (MITs) and East Swan-1 and -2 (LIT).

### 5.1. Fluid flow histories

#### 5.1.1. HIT: Oliver-1

The palaeo-thermometry and palaeo-salinity fluid inclusion data from Oliver-1 were obtained from a sample at 2974.38 m, within the Middle Jurassic Plover Formation reservoir interval. This zone in Oliver-1 is presently near the top of a thick, gas-bearing interval, though other fluid inclusion studies (O'Brien et al., 1996b) have shown that it lies within a pre-existing oil leg. Homogenisation temperatures ( $T_h$ ) for this interval (Tables 2 and 3) typically range from 100–125 °C, consistent with the present day temperature at this depth (117.2 °C at 3194.0 m). Salinities in the inclusions ( $S_h$ ) vary between 31,990 and 114,090 ppm, again largely consistent with present day salinities within formation water (80,000–90,000 ppm at 3175 m).

#### 5.1.2. MIT: Challis-1

In Challis-1, which is taken to be representative of the Challis oil-field, the Late Triassic reservoir interval is characterised by fluid inclusions with widely varying homogenisation temperatures ( $T_h$ ) and salinities (Tables 2 and 3). Minimum homogenisation temperatures (which are usually considered the most reliable; Eadington et al., 1990), show a systematic increase down the well, from 63 °C (1399–1405 m), through 75 °C (1600–1699 m) to 105 °C between 1861 and 1956 m. Present day temperatures for Challis-1 range from 70 °C (1493 m) to 81 °C (1953 m) and thus the fluid inclusions in the basal samples appear to have been trapped when temperatures were

Table 2

Fluid inclusion data from the wells in the Timor Sea, Australia

Well	Depth (mKB)	Sample type	Formation/age	Mineral	Fluid	Location	T <sub>h</sub> (°C)	T <sub>m</sub> (°C)	Salinity (ppm)
Challis-1	1399–1405	cuttings	Late Triassic	quartz	aqueous	OB	63	nd	
Challis-1	1399–1405	cuttings	Late Triassic	quartz	aqueous	OB	66	nd	
Challis-1	1399–1405	cuttings	Late Triassic	quartz	aqueous	OB	70	nd	
Challis-1	1399–1405	cuttings	Late Triassic	quartz	aqueous	OB	89	nd	
Challis-1	1399–1405	cuttings	Late Triassic	quartz	aqueous	OB	102	nd	
Challis-1	1399–1405	cuttings	Late Triassic	quartz	aqueous	OB	106	nd	
Challis-1	1399–1405	cuttings	Late Triassic	quartz	aqueous	OB	ND	-0.7	12,120
Challis-1	1399–1405	cuttings	Late Triassic	quartz	aqueous	FO	125	-1.5	25,490
Challis-1	1399–1405	cuttings	Late Triassic	quartz	aqueous	FO	>130	-3.4	55,250
Challis-1	1399–1405	cuttings	Late Triassic	quartz	aqueous	FO	ND	-2.8	46,150
Challis-1	1399–1405	cuttings	Late Triassic	quartz	aqueous	FO	ND	-2.5	41,500
Challis-1	1399–1405	cuttings	Late Triassic	quartz	aqueous	FO	ND	-0.8	13,820
Challis-1	1600–99	cuttings	Late Triassic	quartz	aqueous	OB	75	nd	
Challis-1	1600–99	cuttings	Late Triassic	quartz	aqueous	OB	75	nd	
Challis-1	1600–99	cuttings	Late Triassic	quartz	aqueous	OB	78	nd	
Challis-1	1600–99	cuttings	Late Triassic	quartz	aqueous	OB	78	nd	
Challis-1	1600–99	cuttings	Late Triassic	quartz	aqueous	OB	85	-3.5	56,740
Challis-1	1600–99	cuttings	Late Triassic	quartz	aqueous	OB	125	nd	
Challis-1	1600–99	cuttings	Late Triassic	quartz	aqueous	OB	>125	-2.6	43,050
Challis-1	1600–99	cuttings	Late Triassic	quartz	aqueous	OB	ND	-23	232,930
Challis-1	1600–99	cuttings	Late Triassic	quartz	aqueous	OB	ND	-3.5	56,740
Challis-1	1600–99	cuttings	Late Triassic	quartz	aqueous	OB	ND	-5.6	86,350
Challis-1	1861–1956	cuttings	Late Triassic	quartz	aqueous	OB	105	nd	
Challis-1	1600–99	cuttings	Late Triassic	quartz	aqueous	OB	106	-1.5	25,490
Challis-1	1600–99	cuttings	Late Triassic	quartz	aqueous	OB	>124	-9.5	133,370
Challis-1	1600–99	cuttings	Late Triassic	quartz	aqueous	OB	>124	-6.2	94,240
Challis-1	1600–99	cuttings	Late Triassic	quartz	aqueous	OB	111	nd	
East Swan-2	1130	cuttings	Grebe Formation	quartz	aqueous	OB	>120	-3.6	58,220
East Swan-2	1130	cuttings	Grebe Formation	quartz	aqueous	OB	>120	-5.3	82,310
East Swan-2	1130	cuttings	Grebe Formation	quartz	aqueous	OB	>120	-8.3	119,950
East Swan-2	1130	cuttings	Grebe Formation	quartz	aqueous	OB	>120	-3.3	53,750
East Swan-2	1130	cuttings	Grebe Formation	quartz	aqueous	OB	>120	nd	
East Swan-2	1130	cuttings	Grebe Formation	quartz	aqueous	OB	>120	-16.3	193,970
East Swan-2	1130	cuttings	Grebe Formation	quartz	aqueous	OB	>120	-17.2	200,250
East Swan-2	1130	cuttings	Grebe Formation	quartz	aqueous	OB	>120	-1.3	22,200
East Swan-2	1130	cuttings	Grebe Formation	quartz	aqueous	OB	>120	-17	198,890
East Swan-2	1130	cuttings	Grebe Formation	quartz	aqueous	OB	>120	-1.9	31,990
East Swan-2	1130	cuttings	Grebe Formation	quartz	aqueous	OB	>120	-2.3	38,360
East Swan-2	1130	cuttings	Grebe Formation	quartz	aqueous	OB	>120	-2.2	36,770
East Swan-2	1130	cuttings	Grebe Formation	quartz	aqueous	OB	>120	-6.5	98,090
East Swan-2	1130	cuttings	Grebe Formation	quartz	aqueous	FCO	88	-8	116,450
East Swan-2	1220	cuttings	Grebe Formation	quartz	aqueous	OB	58	nd	
East Swan-2	1220	cuttings	Grebe Formation	quartz	aqueous	OB	76	nd	
East Swan-2	1220	cuttings	Grebe Formation	quartz	aqueous	OB	60	nd	
East Swan-2	1220	cuttings	Grebe Formation	quartz	aqueous	OB	>120	-26.5	247,330
East Swan-2	1220	cuttings	Grebe Formation	quartz	aqueous	OB	>120	nd	
East Swan-2	1220	cuttings	Grebe Formation	quartz	aqueous	OB	>120	nd	
East Swan-2	1220	cuttings	Grebe Formation	quartz	aqueous	OB	>120	-14.8	182,670
East Swan-2	1220	cuttings	Grebe Formation	quartz	aqueous	OB	>120	nd	
East Swan-2	1220	cuttings	Grebe Formation	quartz	aqueous	OB	>120	-16.4	194,690
East Swan-2	1220	cuttings	Grebe Formation	quartz	aqueous	OB	>120	-23.4	234,750
East Swan-2	1220	cuttings	Grebe Formation	quartz	aqueous	OB	>120	-10	138,700
East Swan-2	1220	cuttings	Grebe Formation	quartz	aqueous	OB	>120	-19.2	212,970
East Swan-2	1220	cuttings	Grebe Formation	quartz	aqueous	OB	>120	nd	
East Swan-2	1220	cuttings	Grebe Formation	quartz	aqueous	OB	>120	nd	
East Swan-2	1220	cuttings	Grebe Formation	quartz	aqueous	OB	>120	nd	
East Swan-2	1220	cuttings	Grebe Formation	quartz	aqueous	OB	>120	-3.3	53,750

continued.

Table 2 (continued)

Well	Depth (mKB)	Sample type	Formation/age	Mineral	Fluid	Location	$T_h$ (°C)	$T_m$ (°C)	Salinity (ppm)
East Swan-2	1220	cuttings	Grebe Formation	quartz	aqueous	OB	>120	nd	nd
East Swan-2	1220	cuttings	Grebe Formation	quartz	aqueous	OB	>120	-1.9	31,990
East Swan-2	1220	cuttings	Grebe Formation	quartz	aqueous	OB	>120	-1.3	22,200
East Swan-2	1290	cuttings	Grebe Formation	quartz	aqueous	OB	>120	-17.5	202,270
East Swan-2	1290	cuttings	Grebe Formation	quartz	aqueous	OB	>120	-18.5	208,700
East Swan-2	1290	cuttings	Grebe Formation	quartz	aqueous	OB	>120	-13.7	173,680
East Swan-2	1290	cuttings	Grebe Formation	quartz	aqueous	OB	>120	nd	nd
East Swan-2	1290	cuttings	Grebe Formation	quartz	aqueous	OB	>120	-19.8	216,460
East Swan-2	1290	cuttings	Grebe Formation	quartz	aqueous	OB	>120	-2	33,590
East Swan-2	1290	cuttings	Grebe Formation	quartz	aqueous	OB	>120	-1.8	30,370
East Swan-2	1290	cuttings	Grebe Formation	quartz	aqueous	OB	>120	-2	33,590
East Swan-2	1290	cuttings	Grebe Formation	quartz	aqueous	OB	>150	-8.7	124,520
East Swan-2	1290	cuttings	Grebe Formation	quartz	aqueous	FCO	>120	-15.8	190,320

some 25 to perhaps 30°C higher than at present (i.e. 105–110°C).

Fluid inclusion salinities ( $S_{fi}$ ) are low in the upper reservoir units (<55,000 ppm), then display progressive, but erratic, increases down-hole. Salinities in these lower samples overlap the upper units, but samples with very high salinities, occasionally in excess of 230,000 ppm, also occur. These  $S_{fi}$  values greatly exceed the present day salinities in the reservoir at Challis-1 (80,000–90,000 ppm). Significantly, the higher  $S_{fi}$  values are restricted exclusively to below the present day oil–water contact in Challis-1.

The  $T_h$  and  $S_{fi}$  data suggest that the basal reservoir units in Challis-1, located within the present day water zone, have experienced the passage of hot, saline brines (which coincided with the formation of quartz overgrowths and attendant fluid inclusion formation). The fact that salinities are now much lower demonstrates that the flow of these brines has largely, if not completely, ceased.

#### 5.1.3. MIT: Jabiru-1A

Samples were available from four depth intervals within the Middle Jurassic Plover Formation reservoir sands: 1646.4, 1650, 1715 and 1997–2099 m. Minimum  $T_h$  values ranged from 71°C (1646 m), through 74°C (1650 m) to 67°C (1715 m) to 92°C at 1997–2000 m (see Tables 2 and 3; Eadington et al., 1990; Lisk and Eadington, 1994). Temperatures of 65°C at 1669 m and 79°C at 2380 m were recorded in the well. These temperatures are broadly similar to the  $T_h$  values in the shallower intervals (within the present day oil leg), but slightly lower than the  $T_h$  values at depth. The fluid inclusion salinities are typically fairly low (<50,000 ppm) within the present day oil leg, and are in fact lower than present day salinities (60,000–100,000 ppm).

Below the oil leg, however, within the residual oil zone at 1715 m, extremely high salinities were recorded in one

suite of inclusions.  $S_{fi}$  values as high as 277,330 ppm were recorded; in contrast, inclusions within the rest of the fluid inclusions had salinities ranging between 44,600 and 105,620 ppm, again consistent with present day salinities.

The data from Jabiru 1A are consistent with those obtained from Challis-1, and suggest that the reservoir intervals below the present day ‘live’ hydrocarbon columns in the MITs have seen the passage of very saline, relatively high temperature brines.

#### 5.1.4. MIT: Jabiru-2

Two samples were analysed in Jabiru-2, one at 800 m depth within the Eocene Grebe sands and the other at 1664 m depth in the Jurassic Plover Formation. This well contains no live hydrocarbon column and is located within a fluid flow pathway (as defined by the presence of an HRDZ) over the bounding fault of the horst. As such, it provides a potential contrast with Jabiru-1A, which is located in the middle of the horst, away from the bounding faults (Fig. 6).

Two distinct types of fluid inclusions were present in the Plover Formation: inclusions trapped in quartz overgrowths and a younger suite within fractures which cut the overgrowths.

$T_h$  values for the inclusions in the overgrowths range widely, from a minimum of 64 to in excess of 150°C; most values are in the range 80–150°C. In this regard, the temperature data are similar to those from Jabiru-1A. However, salinities in these inclusions range from 69,820 ppm to 220,370 ppm, with the majority being in the range from 150,000–200,000 ppm. These are much more saline than those seen in Jabiru-1A (44,600 and 105,620 ppm).

If the fluid inclusions present in the fractures cutting the overgrowths are considered, the differences between Jabiru-1A and -2 become more striking. These inclusions have salinities consistently in excess of 200,000 ppm, with a maximum value of 249,140 ppm being recorded (range 69,820–249,140 ppm).  $T_h$  varies from a minimum of 109

Table 3

Fluid inclusion data from the wells in the Timor Sea, Australia

Well	Depth (mKB)	Sample type	Formation/age	Mineral	Fluid	Location	T <sub>h</sub> (°C)	T <sub>m</sub> (°C)	Salinity (ppm)
Jabiru-1A	1646.4	core	Plover Formation	quartz	oil	OB	71	nd	nd
Jabiru-1A	1646.4	core	Plover Formation	quartz	oil	OB	73	nd	nd
Jabiru-1A	1646.4	core	Plover Formation	quartz	oil	OB	73	nd	nd
Jabiru-1A	1646.4	core	Plover Formation	quartz	oil	OB	87	nd	nd
Jabiru-1A	1646.4	core	Plover Formation	quartz	oil	OB	89	nd	nd
Jabiru-1A	1646.4	core	Plover Formation	quartz	oil	OB	101	nd	nd
Jabiru-1A	1646.4	core	Plover Formation	quartz	oil	OB	>110	nd	nd
Jabiru-1A	1646.4	core	Plover Formation	quartz	oil	OB	>110	nd	nd
Jabiru-1A	1650	core	Plover Formation	quartz	aqueous	OB	74	-1	17,190
Jabiru-1A	1650	core	Plover Formation	quartz	oil	OB	76	nd	nd
Jabiru-1A	1650	core	Plover Formation	quartz	oil	OB	77	nd	nd
Jabiru-1A	1650	core	Plover Formation	quartz	aqueous	OB	78	-1.2	20,540
Jabiru-1A	1650	core	Plover Formation	quartz	oil	OB	79	nd	nd
Jabiru-1A	1650	core	Plover Formation	quartz	oil	OB	81	nd	nd
Jabiru-1A	1650	core	Plover Formation	quartz	oil	OB	86	nd	nd
Jabiru-1A	1650	core	Plover Formation	quartz	oil	OB	89	nd	nd
Jabiru-1A	1650	core	Plover Formation	quartz	aqueous	OB	95	-1.4	23,850
Jabiru-1A	1650	core	Plover Formation	quartz	aqueous	OB	96	1	nd
Jabiru-1A	1650	core	Plover Formation	quartz	oil	OB	96	nd	nd
Jabiru-1A	1650	core	Plover Formation	quartz	aqueous	OB	97	-2.1	35,190
Jabiru-1A	1650	core	Plover Formation	quartz	oil	OB	103	nd	nd
Jabiru-1A	1650	core	Plover Formation	quartz	oil	OB	103	nd	nd
Jabiru-1A	1650	core	Plover Formation	quartz	oil	OB	105	nd	nd
Jabiru-1A	1650	core	Plover Formation	quartz	oil	OB	108	nd	nd
Jabiru-1A	1650	core	Plover Formation	quartz	aqueous	OB	110	nd	nd
Jabiru-1A	1650	core	Plover Formation	quartz	oil	OB	112	nd	nd
Jabiru-1A	1650	core	Plover Formation	quartz	oil	OB	>120	nd	nd
Jabiru-1A	1650	core	Plover Formation	quartz	aqueous	OB	>120	-2.9	47,680
Jabiru-1A	1650	core	Plover Formation	quartz	aqueous	OB	>120	-2.8	46,150
Jabiru-1A	1650	core	Plover Formation	quartz	aqueous	OB	>120	-1.5	25,490
Jabiru-1A	1650	core	Plover Formation	quartz	aqueous	OB	>120	-1.9	31,990
Jabiru-1A	1650	core	Plover Formation	quartz	aqueous	OB	nd	-3	49,210
Jabiru-1A	1650	core	Plover Formation	quartz	aqueous	OB	nd	-0.5	8,700
Jabiru-1A	1650	core	Plover Formation	quartz	aqueous	OB	nd	-1.5	25,490
Jabiru-1A	1650	core	Plover Formation	quartz	aqueous	OB	nd	-2.5	41,500
Jabiru-1A	1650	core	Plover Formation	quartz	aqueous	OB	nd	-1.8	30,370
Jabiru-1A	1715	cuttings	Plover Formation	quartz	aqueous	IOB	67	nd	nd
Jabiru-1A	1715	cuttings	Plover Formation	quartz	aqueous	IOB	75	-36	274,870
Jabiru-1A	1715	cuttings	Plover Formation	quartz	aqueous	IOB	78	-37	277,330
Jabiru-1A	1715	cuttings	Plover Formation	quartz	aqueous	IOB	81	nd	nd
Jabiru-1A	1715	cuttings	Plover Formation	quartz	aqueous	IOB	84	nd	nd
Jabiru-1A	1715	cuttings	Plover Formation	quartz	aqueous	IOB	103	nd	nd
Jabiru-1A	1715	cuttings	Plover Formation	quartz	aqueous	IOB	106	nd	nd
Jabiru-1A	1715	cuttings	Plover Formation	quartz	aqueous	IOB	117	nd	nd
Jabiru-1A	1715	cuttings	Plover Formation	quartz	aqueous	IOB	123	nd	nd
Jabiru-1A	1715	cuttings	Plover Formation	quartz	aqueous	IOB	142	nd	nd
Jabiru-1A	1715	cuttings	Plover Formation	quartz	aqueous	IOB	>120	-17	198,890
Jabiru-1A	1715	cuttings	Plover Formation	quartz	aqueous	IOB	>120	-17.3	200,930
Jabiru-1A	1715	cuttings	Plover Formation	quartz	aqueous	IOB	nd	-35.5	273,630
Jabiru-1A	1715	cuttings	Plover Formation	quartz	aqueous	IOB	nd	-6.4	96,820
Jabiru-1A	1715	cuttings	Plover Formation	quartz	aqueous	IOB	nd	-7	104,380
Jabiru-1A	1715	cuttings	Plover Formation	quartz	aqueous	OB	70	nd	nd
Jabiru-1A	1715	cuttings	Plover Formation	quartz	aqueous	OB	70	nd	nd
Jabiru-1A	1715	cuttings	Plover Formation	quartz	aqueous	OB	70	-6	91,640
Jabiru-1A	1715	cuttings	Plover Formation	quartz	aqueous	OB	71	-2.9	47,680
Jabiru-1A	1715	cuttings	Plover Formation	quartz	aqueous	OB	71	nd	nd
Jabiru-1A	1715	cuttings	Plover Formation	quartz	aqueous	OB	72	-7.1	105,620
Jabiru-1A	1715	cuttings	Plover Formation	quartz	aqueous	OB	73	-2.7	44,600
Jabiru-1A	1715	cuttings	Plover Formation	quartz	aqueous	OB	73	-3.3	53,750
Jabiru-1A	1715	cuttings	Plover Formation	quartz	aqueous	OB	73	nd	nd

continued.

Table 3 (continued)

Well	Depth (mKB)	Sample type	Formation/age	Mineral	Fluid	Location	T <sub>b</sub> (°C)	T <sub>m</sub> (°C)	Salinity (ppm)
Jabiru-1A	1715	cuttings	Plover Formation	quartz	aqueous	OB	74	-6	91,640
Jabiru-1A	1715	cuttings	Plover Formation	quartz	aqueous	OB	75	-6	91,640
Jabiru-1A	1715	cuttings	Plover Formation	quartz	aqueous	OB	77	-6	91,640
Jabiru-1A	1715	cuttings	Plover Formation	quartz	aqueous	OB	77	-6.6	99,360
Jabiru-1A	1715	cuttings	Plover Formation	quartz	aqueous	OB	77	-7	104,380
Jabiru-1A	1715	cuttings	Plover Formation	quartz	aqueous	OB	81	-6	91,640
Jabiru-2	1664	cuttings	Plover Formation	quartz	aqueous	OB	68	-13.5	171,980
Jabiru-2	1664	cuttings	Plover Formation	quartz	aqueous	OB	64	-18	205,540
Jabiru-2	1664	cuttings	Plover Formation	quartz	aqueous	OB	66	nd	nd
Jabiru-2	1664	cuttings	Plover Formation	quartz	aqueous	OB	67	nd	nd
Jabiru-2	1664	cuttings	Plover Formation	quartz	aqueous	OB	67	nd	nd
Jabiru-2	1664	cuttings	Plover Formation	quartz	aqueous	OB	67	nd	nd
Jabiru-2	1664	cuttings	Plover Formation	quartz	aqueous	OB	68	nd	nd
Jabiru-2	1664	cuttings	Plover Formation	quartz	aqueous	OB	68	nd	nd
Jabiru-2	1664	cuttings	Plover Formation	quartz	aqueous	OB	72	-10	138,700
Jabiru-2	1664	cuttings	Plover Formation	quartz	aqueous	OB	76	nd	nd
Jabiru-2	1664	cuttings	Plover Formation	quartz	aqueous	OB	80	-13	167,640
Jabiru-2	1664	cuttings	Plover Formation	quartz	aqueous	OB	89	nd	nd
Jabiru-2	1664	cuttings	Plover Formation	quartz	aqueous	OB	109	-18	205,540
Jabiru-2	1664	cuttings	Plover Formation	quartz	aqueous	OB	111	-20.5	220,370
Jabiru-2	1664	cuttings	Plover Formation	quartz	aqueous	OB	127	nd	nd
Jabiru-2	1664	cuttings	Plover Formation	quartz	aqueous	OB	135	-17.5	202,270
Jabiru-2	1664	cuttings	Plover Formation	quartz	aqueous	OB	143	-12.5	163,160
Jabiru-2	1664	cuttings	Plover Formation	quartz	aqueous	OB	150	-16	191,800
Jabiru-2	1664	cuttings	Plover Formation	quartz	aqueous	OB	150	-4.5	71,230
Jabiru-2	1664	cuttings	Plover Formation	quartz	aqueous	OB	150	-4.7	74,050
Jabiru-2	1664	cuttings	Plover Formation	quartz	aqueous	OB	150	-4.6	72,640
Jabiru-2	1664	cuttings	Plover Formation	quartz	aqueous	OB	150	-4.4	69,820
Jabiru-2	1664	cuttings	Plover Formation	quartz	aqueous	OB	150	nd	nd
Jabiru-2	1664	cuttings	Plover Formation	quartz	aqueous	OB	150	-5.3	82,310
Jabiru-2	1664	cuttings	Plover Formation	quartz	aqueous	FCO	109	-20.5	220,370
Jabiru-2	1664	cuttings	Plover Formation	quartz	aqueous	FCO	120	-25	241,560
Jabiru-2	1664	cuttings	Plover Formation	quartz	aqueous	FCO	125	-18	205,540
Jabiru-2	1664	cuttings	Plover Formation	quartz	aqueous	FCO	125	-20.5	220,370
Jabiru-2	1664	cuttings	Plover Formation	quartz	aqueous	FCO	126	-22	228,160
Jabiru-2	1664	cuttings	Plover Formation	quartz	aqueous	FCO	131	-16	191,800
Jabiru-2	1664	cuttings	Plover Formation	quartz	aqueous	FCO	131	-20.5	220,370
Jabiru-2	1664	cuttings	Plover Formation	quartz	aqueous	FCO	133	-27	249,140
Jabiru-2	1664	cuttings	Plover Formation	quartz	aqueous	FCO	144	-22.5	230,580
Jabiru-2	1664	cuttings	Plover Formation	quartz	aqueous	FCO	146	-19.5	214,730
Jabiru-2	1664	cuttings	Plover Formation	quartz	aqueous	FCO	147	-13	167,640
Jabiru-2	1664	cuttings	Plover Formation	quartz	aqueous	FCO	150	-18	205,540
Jabiru-2	1664	cuttings	Plover Formation	quartz	aqueous	FCO	150	-17.5	202,270
Jabiru-2	1664	cuttings	Plover Formation	quartz	aqueous	FCO	150	-20	217,600
Jabiru-2	1664	cuttings	Plover Formation	quartz	aqueous	FCO	150	-20.1	218,160
Jabiru-2	1664	cuttings	Plover Formation	quartz	aqueous	FCO	150	-12	158,550
Jabiru-2	1664	cuttings	Plover Formation	quartz	aqueous	FCO	150	nd	nd
Jabiru-2	1664	cuttings	Plover Formation	quartz	aqueous	FCO	150	nd	nd
Jabiru-2	1664	cuttings	Plover Formation	quartz	aqueous	FCO	160	-26	245,470
Jabiru-2	800	cuttings	Grebe Formation	quartz	aqueous	OB	83	nd	nd
Jabiru-2	800	cuttings	Grebe Formation	quartz	aqueous	OB	85	-5.9	90,330
Jabiru-2	800	cuttings	Grebe Formation	quartz	aqueous	OB	87	nd	nd
Jabiru-2	800	cuttings	Grebe Formation	quartz	aqueous	OB	89	-5.5	85,010
Jabiru-2	800	cuttings	Grebe Formation	quartz	aqueous	OB	90	-27	249,140
Jabiru-2	800	cuttings	Grebe Formation	quartz	aqueous	OB	94	-9	127,890
Jabiru-2	800	cuttings	Grebe Formation	quartz	aqueous	OB	103	nd	nd
Jabiru-2	800	cuttings	Grebe Formation	quartz	aqueous	OB	107	nd	nd
Jabiru-2	800	cuttings	Grebe Formation	quartz	aqueous	OB	107	-9	127,890
Jabiru-2	800	cuttings	Grebe Formation	quartz	aqueous	OB	109	nd	nd
Jabiru-2	800	cuttings	Grebe Formation	quartz	aqueous	OB	124	-6.8	101,880

continued.

Table 3 (continued)

Well	Depth (mKB)	Sample type	Formation/age	Mineral	Fluid	Location	$T_h$ (°C)	$T_m$ (°C)	Salinity (ppm)
Jabiru-2	800	cuttings	Grebe Formation	quartz	aqueous	OB	125	nd	nd
Jabiru-2	800	cuttings	Grebe Formation	quartz	aqueous	OB	130	-29	255,830
Jabiru-2	800	cuttings	Grebe Formation	quartz	aqueous	OB	139	nd	nd
Jabiru-2	800	cuttings	Grebe Formation	quartz	aqueous	OB	142	-18	205,540
Jabiru-2	800	cuttings	Grebe Formation	quartz	aqueous	OB	144	-25	241,560
Jabiru-2	800	cuttings	Grebe Formation	quartz	aqueous	OB	>150	-7.2	106,850
Jabiru-2	800	cuttings	Grebe Formation	quartz	aqueous	OB	>150	-8.6	123,390
Jabiru-2	800	cuttings	Grebe Formation	quartz	aqueous	OB	>150	-8.6	123,390
Jabiru-2	800	cuttings	Grebe Formation	quartz	aqueous	OB	>150	-7.2	106,850
Jabiru-2	800	cuttings	Grebe Formation	quartz	aqueous	OB	>150	-19	211,770
Jabiru-2	800	cuttings	Grebe Formation	quartz	aqueous	OB	>150	nd	nd
Jabiru-2	800	cuttings	Grebe Formation	quartz	aqueous	OB	>150	nd	nd
Jabiru-2	800	cuttings	Grebe Formation	quartz	aqueous	OB	nd	-10.5	143,880
Jabiru-2	800	cuttings	Grebe Formation	quartz	aqueous	WO	111	-4	64,080
Jabiru-2	800	cuttings	Grebe Formation	quartz	aqueous	WO	123	nd	nd
Jabiru-2	800	cuttings	Grebe Formation	quartz	aqueous	FCO	111	nd	nd
Oliver-1	2974.38	core	Plover Formation	quartz	aqueous	OB	100	-4.2	66,960
Oliver-1	2974.38	core	Plover Formation	quartz	aqueous	OB	101	-5.5	85,010
Oliver-1	2974.38	core	Plover Formation	quartz	aqueous	OB	104	-3.4	55,250
Oliver-1	2974.38	core	Plover Formation	quartz	aqueous	OB	104	-2.1	35,190
Oliver-1	2974.38	core	Plover Formation	quartz	aqueous	OB	105	-3.3	53,750
Oliver-1	2974.38	core	Plover Formation	quartz	aqueous	OB	106	-5.7	87,680
Oliver-1	2974.38	core	Plover Formation	quartz	aqueous	OB	106	-6.5	98,090
Oliver-1	2974.38	core	Plover Formation	quartz	aqueous	OB	106	-6.5	98,090
Oliver-1	2974.38	core	Plover Formation	quartz	aqueous	OB	108	-2.4	39,930
Oliver-1	2974.38	core	Plover Formation	quartz	aqueous	OB	108	-6.5	nd
Oliver-1	2974.38	core	Plover Formation	quartz	aqueous	OB	109	-7.8	114,090
Oliver-1	2974.38	core	Plover Formation	quartz	aqueous	OB	110	-6.9	103,140
Oliver-1	2974.38	core	Plover Formation	quartz	aqueous	OB	113	-7	104,380
Oliver-1	2974.38	core	Plover Formation	quartz	aqueous	OB	114	-6.8	101,880
Oliver-1	2974.38	core	Plover Formation	quartz	aqueous	OB	115	-6.4	96,820
Oliver-1	2974.38	core	Plover Formation	quartz	aqueous	OB	118	-7	104,380
Oliver-1	2974.38	core	Plover Formation	quartz	aqueous	OB	124	-1.9	31,990
Oliver-1	2974.38	core	Plover Formation	quartz	aqueous	OB	125	-4.2	66,960
Oliver-1	2974.38	core	Plover Formation	quartz	aqueous	OB	>150	nd	nd
Oliver-1	2974.38	core	Plover Formation	quartz	aqueous	OB	nd	-7.3	108,070

to  $>150^\circ\text{C}$ . The  $T_h$  minimum value is  $\sim 35^\circ\text{C}$  higher than the present day well-bore temperature at this depth ( $76^\circ\text{C}$  at 1683 m). The later fluids were hotter and perhaps more saline than those responsible for the inclusions in the overgrowths.

The quartz overgrowths from the Grebe sands in Jabiru-2 yielded inclusions with salinities ranging between 64,080 and 255,830 ppm, with most falling in the 100,000–200,000 ppm range.  $T_h$  ranged from  $83^\circ\text{C}$  ( $\sim 43^\circ\text{C}$  higher than the present day well bore temperature) to  $>150^\circ\text{C}$ , with the more saline inclusions being associated with higher temperatures of crystallisation. Unfortunately, circulation was lost through the Grebe sands in Jabiru-1A, so no direct comparison with this well is possible.

The fluid inclusion data from Jabiru-2 support the concept that this well is located on, or close to, a fluid migration pathway. It appears that the fault on which Jabiru-2 lies may be acting effectively as a narrow, linear source, similar to the size of the HRDZ itself ( $200 \times 300$  m),

for the entry of hot and highly saline brines into, and through, the Jabiru structure. *Progressive dilution of the brines away from their source results in both decreasing temperatures and salinities, as evident in Jabiru-1A.* These brines have migrated since the Eocene, as evidence for their passage is present within the Grebe Formation sands. Given that the most saline and highest temperature brines are present within fractures, it is likely that the same tectonic event is responsible for both fracture formation and brine migration (i.e. the Mio-Pliocene event).

#### 5.1.5. LIT: East Swan-2

This well provides additional information on the fluid inclusion characteristics of the Eocene Grebe Formation sands. Lisk (unpublished data) has recognised that quartz overgrowths within the Timor Sea do not usually crystallise at temperatures of  $<50^\circ\text{C}$ . As the Grebe sands are typically at shallow depths of burial and low temperatures throughout the Timor Sea, overgrowths and

attendant fluid inclusions are generally sparse or absent. Exceptions are where the wells have been subjected to abnormally elevated temperatures, such as in zones of active fluid flow.

An HRDZ is well-developed at East Swan-2, and consequently quartz overgrowths containing fluid inclusions are relatively common. The salinity of the fluid inclusions in the three available samples (Tables 2 and 3) ranges from 22,200 to 247,330 ppm, compared to present day salinities in the Grebe sands of 50,000 to 60,000 ppm. Numerous  $S_{fi}$  values in excess of 200,000 ppm were encountered (Tables 2 and 3).

Present day temperatures in the Grebe sands at East Swan-2 are only about 45°C, compared to fluid inclusion homogenisation temperatures which were typically >120°C. Whilst the  $T_h$  could be erroneously high because of the effects of the trapped gas (some of the inclusions contain methane), the data are consistent with the migration of very saline, hot, fluids through the Grebe Formation sands at East Swan-2. Taking the effects of the gas into account, minimum  $T_h$  values of 76 and 88°C were obtained at 1220 and 1130 m, respectively, approximately 30–40°C higher than the present day temperatures. Moreover, the fact that quartz overgrowths (which have trapped the inclusions) are present in such a low temperature (45°C) environment, is evidence that temperatures have been higher in the past.

#### 5.1.6. Discussion of palaeo-temperature and salinity observations

The fluid inclusion data from a number of wells provide evidence that hot, very saline brines have migrated through the Mesozoic and Tertiary sequences in the Timor Sea. The evidence for these brines are best seen close to major fluid flow (fault-controlled) pathways, as defined by the presence of significant HRDZs (e.g. East Swan-2 and Jabiru-2). Further away from these pathways, the brines become increasingly diluted, and both the  $T_h$  and  $S_{fi}$  values fall away.

In wells with 'live' oil legs, such as Challis-1 and Jabiru-1A, the evidence for high salinities and temperatures is restricted to below the present day oil–water contact. This suggests that the brines never penetrated above the OWC in these wells, or perhaps more accurately, they never penetrated into reservoir units containing live columns. Hence, evidence of brine flow may well only be present in the reservoirs of either breached traps or traps that have never been charged, or below the present day OWC (or GWC for that matter) in traps with live columns.

Given that the basal residual columns in the Challis and Jabiru fields did not develop until the Mio-Pliocene fault reactivation, the timing of brine migration can be accurately constrained (<~5.5 Ma). It seems most likely that the margin-scale tectonism which drove the fault

reactivation, and provided the conduits for brine flow, also drove the migration of the brines.

#### 5.2. Thermal histories

The fluid inclusion data have demonstrated that hot, saline brines were migrating through assorted traps within the Timor Sea in the Neogene. Given the apparent high temperature (>100°C) of these brines, they could affect the thermal history of traps through which they passed. As such, apatite fission track analysis (AFTA<sup>®</sup>), which represents a powerful means of analysing the thermal and maturation histories of individual wells, fields and sedimentary basins (Gleadow & Duddy, 1981; Laslett, Kendall, Gleadow, & Duddy, 1982; Laslett, Green, Duddy, & Gleadow, 1987; Gleadow, Duddy, & Lovering, 1983; Gleadow, Duddy, Green, & Lovering, 1986; Green, Duddy, Gleadow, & Lovering, 1989a; Green et al., 1989b; Bray, Green, & Duddy, 1992), has been applied to several wells in the Timor Sea.

The basic principles of AFTA<sup>®</sup> are as follows:

- Igneous apatite contains  $^{238}\text{U}$  which undergoes spontaneous fission at a known rate. This fission induces the formation of fission tracks within the crystal lattice and allows calculation of a fission track 'age'.
- The fission tracks within apatite contained within sedimentary rocks which have not been heated above 50°C have a characteristic distribution of track lengths (mean length 14–15  $\mu\text{m}$ ).
- In samples heated above approximately 50°C, progressive annealing of the tracks takes place, with the track lengths shortening to 'zero' (complete annealing) at about 120°C. As such, the annealing temperatures of apatite are very similar to the thermal maturation range of hydrocarbon source rocks. Complex basin histories can be reconstructed from this effect. For example, rapid subsidence and heating to ~100°C would shorten existing tracks significantly. However, if the basin or well location were then uplifted (and as a result cooled), all subsequently formed tracks at a given depth would be longer than the pre-existing tracks (which had been subject to the increased thermal regime). As such, a bimodal fission track distribution would be present. In basins/wells with more simple burial histories (continuous burial), apatite fission track lengths show a more unimodal distribution, with track lengths and fission track 'ages' both decreasing with increasing depth in the basin/well.

Modelling of the apatite 'age' and the fission track length and distribution can thus allow reconstruction of the thermal and uplift/subsidence histories of basins. AFTA<sup>®</sup> is also particularly useful in assessing transient thermal effects due to fluid flow. Modelling of transient thermal pulses, particularly when constrained by other data such as fluid inclusion measurements, can constrain

the duration, temperature and geologic age of a given fluid movement. In this paper, the AFTA<sup>®</sup> modelling has incorporated a number of other data, including bottom hole temperature, vitrinite reflectance and fluid inclusion data, to further characterise the nature and effects of the Late Tertiary fluid flow event. The modelling procedures used have been described previously by Green et al. (1989b) and Duddy, Green, Bray and Hegarty (1994) and Duddy, Green, Hegarty, Bray and O'Brien (1997).

The wells investigated using AFTA<sup>®</sup> were Oliver-1 (HIT), Challis-1, Jabiru-1A and -2 (MITs), and East Swan-1 and -2 (LIT). The observations were as follows.

#### 5.2.1. HIT: Oliver-1

The AFTA<sup>®</sup> results for Oliver-1 (Geotrack, 1988) are summarised in Fig. 9a. There is a progressive decrease in apatite ages with increasing downhole temperature (depth), and a good match between the available AFTA<sup>®</sup> data and the present day temperature profile (using a geothermal gradient of  $\sim 32^{\circ}\text{C}/\text{km}$ , based upon corrected BHT data). In the Tertiary (Miocene and Eocene) and Late Cretaceous section, the ages are greater than, or equal to, the stratigraphic age, whereas in the Jurassic sequences, the AFTA<sup>®</sup> ages are less than the stratigraphic ages, and approach zero as the present day temperature nears  $120^{\circ}\text{C}$ . The AFTA<sup>®</sup> data indicate that the sequences in Oliver-1 have had a relatively simple burial history, free from periods of significant uplift and erosion, and are now at their maximum temperature.

The results from Oliver-1 are consistent with AFTA<sup>®</sup> data obtained from Montara-1, another HIT (O'Brien et al., 1996b). As such, neither Oliver-1 nor Montara-1 show any evidence for the passage of hot brines in the Miocene-Pliocene, consistent with fluid inclusion data.

#### 5.2.2. MIT: Challis-1

The AFTA<sup>®</sup> data for Challis-1 (Geotrack, 1987) are shown in Fig. 9b, and contrast sharply with those from Oliver-1. Challis-1 shows an extremely complex thermal history and both the fission track ages and track lengths decrease fairly consistently up the well. The samples which give the oldest AFTA<sup>®</sup> ages are located within the Ladinian (Middle Triassic) reservoir section, in spite of the fact that the present day temperature at this depth is  $\sim 100^{\circ}\text{C}$ . There is also strong variability in the AFTA<sup>®</sup> ages within the Triassic reservoir interval, with the youngest AFTA<sup>®</sup> ages being obtained from the top of the reservoir. Paradoxically, the youngest AFTA<sup>®</sup> age comes from the shallowest sample (Maastrichtian; 1040–1090 m), which is experiencing present day temperatures of only about  $\sim 52^{\circ}\text{C}$ . The AFTA<sup>®</sup> data suggest that the Ladinian to Maastrichtian samples ( $\sim 1040$  to 1714 m) in Challis-1 have experienced palaeo-temperatures approximately 30–60°C hotter than those at the present day.

The AFTA<sup>®</sup> profiles in Challis-1 can not be explained by either higher palaeo-geothermal gradients or greater burial (prior to uplift and erosion), as both of these effects produce a downward increase in maximum palaeo-tem-

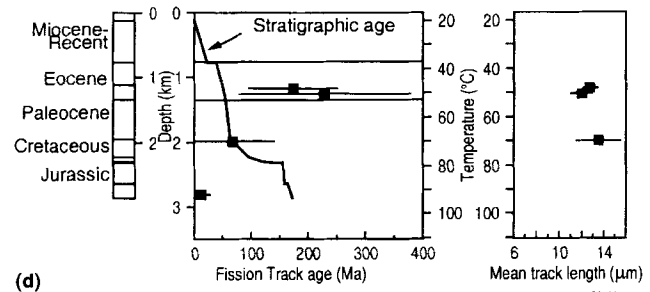
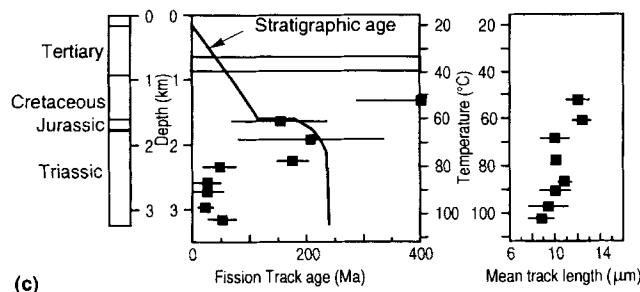
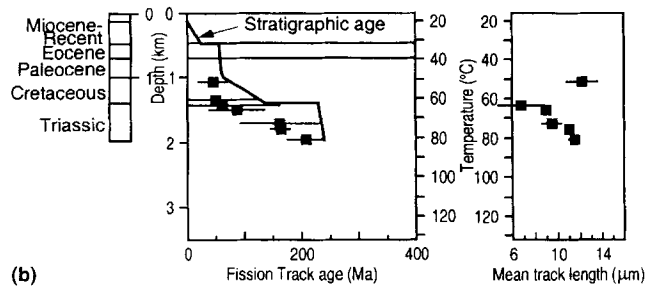
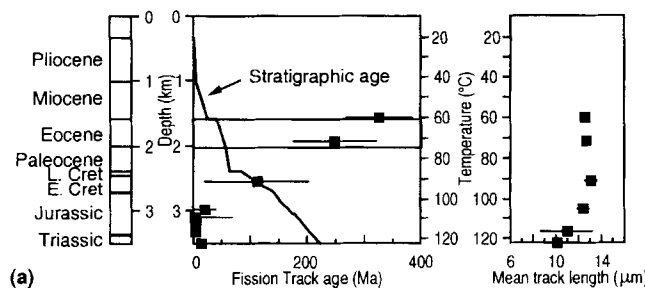


Fig. 9. AFTA<sup>®</sup> parameters plotted against sample depth and present temperature for samples from assorted wells in the Timor Sea. (a) Oliver-1 (high integrity trap), (b) Challis-1 (moderate integrity trap), (c) Jabiru-1A (moderate integrity trap) and (d) East Swan-2 (low integrity trap).

perature, the opposite of what is observed. As such, and considering the fluid inclusion results, the preferred explanation for the AFTA<sup>R</sup> profiles shown in Fig. 9 is that hot (90–120°C) fluids have passed through the section intersected by the Challis-1 well.

Modelling of the shape of the profile, using techniques outlined in Ziagos and Blackwell (1986), suggests that this fluid flow event lasted for less than one million years (Fig. 10). The fact that some of the Triassic sands show the effects of fluid flow quite clearly, and others do not, indicates that the fluid flow was localised, perhaps because of variations in reservoir permeability, the presence of permeability barriers, or local faulting (assuming the fluid flow is mostly fault-controlled).

The exact timing of the transient fluid flow event cannot be constrained, because of limited sample availability. However, the best-fit estimate on the timing from the

AFTA<sup>R</sup> results suggests that a Late Tertiary timing for the fluid migration, probably within the last five million years, but clearly within the last 10 Ma. This is consistent with the evidence from the fluid inclusion  $T_h$  data for a Mio-Pliocene fluid flow event.

### 5.2.3. MIT: Jabiru-1A and -2

The apparent age and mean track length data for Jabiru-1A (Geotrack, 1987) show a general decrease (Fig. 9c) with increasing depth (i.e. with increasing down-hole temperature). Several samples deviate from this trend, however. The shallowest reliable sample (Hettangian; 1637 m) has a much younger AFTA<sup>R</sup> age (38 Ma) than its stratigraphic age (~204 Ma). To produce this difference would require heating to about 90°C, compared to its present day temperature of 63°C. Similar arguments apply to most of the samples in the Triassic sands below the Jurassic reservoirs. These samples, which range from depths of 1910–2972 m, corresponding to present day temperatures between ~71 and 101°C, consistently require heating to temperatures of 90–100°C to produce their respective fission track ages and lengths. The deepest sample (3159 m) is the only one in which there is good agreement between the fission track ages and lengths, and the present day temperature (~106°C).

As with Challis-1, the data from Jabiru-1A support the concept of localised, late stage, hot fluids migrating through the reservoir and younger section.

A single AFTA<sup>R</sup> sample was taken from the Grebe Formation in Jabiru-2, a well drilled through a major fluid flow pathway (i.e. an HRDZ). The results were broadly consistent to those obtained from the deeper intervals in Jabiru-1A.

### 5.2.4. LIT: East Swan-2

On the basis of the location of East Swan-2 within a major fluid flow pathway (i.e. an HRDZ), and considering the results obtained from the MITs (above), it was expected that East Swan-2 would show evidence of the passage of hot fluids in its AFTA<sup>R</sup> results. The fission track data (Fig. 12), however, show that the samples are dominated by the inheritance of ages from the source terrain (300–400 Ma), which are well in excess of the fission track ages for many of the deeper samples in the MITs (Geotrack, 1997). Both the length and the age of the fission tracks increase with increasing downhole temperature, and show no direct evidence for localised heating shallow in the section.

Kinetic modelling of the AFTA<sup>R</sup> data (Fig. 10) from the Grebe Formation, the locus of HRDZ formation in East Swan-2, shows that maximum palaeo-temperatures in the Late Tertiary cannot have exceeded 90°C for any significant time interval period. The modelling constrains the duration of any transient heat events to less than 100,000 years, with the majority of the data suggesting that maximum palaeo-temperatures were less than 80°C.

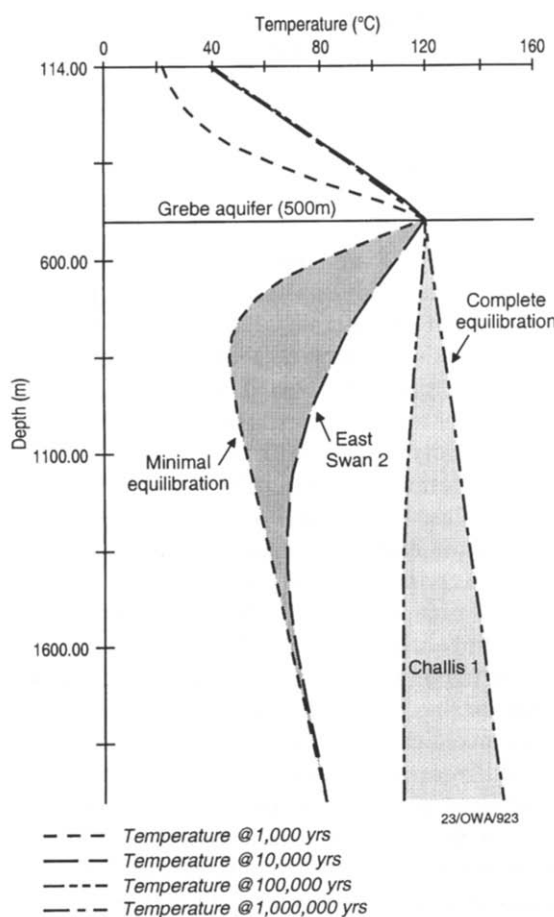


Fig. 10. A theoretical representation of the temperature profiles produced around a generic Eocene aquifer at ~500 m depth, carrying a fluid with a temperature of ~120°C, for flow durations ranging between 1000 and 1,000,000 years. Complete equilibration of the fission tracks with the transient heating resulting from hot fluid flow takes place once the duration of the flow reaches 1,000,000 years. Lesser flow durations result in partial equilibration. Duration of the transient heating events calculated from the AFTA<sup>R</sup> data for the MITs (represented by Challis-1) and LITs (represented by East Swan-2) wells are indicated. Similar results were obtained using fluid temperatures of 90°C.

Whilst these values are in excess of the present day temperatures (73.7°C at 1750 m), there is no direct evidence in the AFTA® data from East Swan-2 of any sustained, hot, fluid flow event. In some ways, the East Swan AFTA® data bear more similarities to those obtained from the Oliver or Montara wells, rather than Challis-1 or Jabiru-1A.

#### 5.2.5. Discussion of Timor Sea AFTA® data

The available AFTA® data indicate that high integrity traps, such as Oliver-1, reached their maximum temperatures at the present day, and have not experienced any transient events involving the passage of hot (90–120°C) fluids. In contrast, moderate integrity traps, such as Challis and Jabiru, show evidence that localised, hot fluids have flowed through them in the Late Tertiary. The best estimate for the timing of the passage of these fluids would be latest Miocene to Early Pliocene, contemporaneous with the reactivation event which led to the breaching of many traps in this region. The corollary of this is that the hot, saline brines, the evidence for which is seen in the fluid inclusions, were responsible for the thermal effects apparent in the AFTA® data.

The breached trap tested by the East Swan-1 and -2 wells contained compelling fluid inclusion evidence for the passage of very saline, and apparently hot, brines in the Late Miocene/Early Pliocene. In spite of this, East Swan-2 showed no AFTA® evidence for sustained, hot, fluid migration. The best way of reconciling the AFTA® and fluid inclusion data is that the total period of brine flow was much shorter at East Swan compared to Challis and Jabiru.

This requirement relates to the kinetics of fission track annealing. Modelling of palaeo-temperature profiles for transient heating within a generic Grebe Formation aquifer sand (Fig. 10) at approximately 500 m depth (the approximate depth of the Grebe Formation throughout the Timor Sea in the latest Miocene/Early Pliocene), and kinetic modelling of AFTA® (and also vitrinite) data throughout the whole of the East Swan-2 well, suggests that the duration of heating (i.e. hot fluid flow) would have to have been very much less than 100,000 and perhaps even less than 10,000 years. This compares to fluid flow durations of 100,000–1,000,000 years for the MITs (Figs. 10 and 11). *These data effectively constrain the period of time during reactivation during which the faults were strongly 'open' or dilatational in the MITs and LITs.*

Perhaps these observations can be explained by the fact that the LITs are typically massively fault-reactivated, whereas the MITs are much less so. Traps such as Challis and Jabiru could have leaked relatively smaller amounts of brine through narrow, focussed fault arrays over a much longer period of time, producing a prominent thermal effect in the process. In contrast, LITs appear to have experienced the leakage of large volumes of brines through a massive fault network for a relatively short

amount of time. These observations actually suggest that the total amount of brine available for transport is finite. The HITs, lacking suitable dilatational fault networks, lacked the conduits necessary for brine migration from depth.

#### 5.3. Determining the source of the brines

The most likely source of the brines which have been trapped in the fluid inclusions, and which produced the thermal effects, is the Siluro-Ordovician evaporites which have been inferred to underlie widespread areas of the Timor Sea (O'Brien et al., 1993, 1996a). These evaporites have produced salt diapirs at a number of locations which have been drilled (eg., Sandpiper-1; Paqualin-1). In order to characterise the origin of the brines, and to better understand any mixing processes which took place between the brines and the connate waters within the Grebe aquifer, strontium, carbon and oxygen stable isotope data were acquired and analysed. The results are presented below.

##### 5.3.1. Carbon and oxygen isotope data

Carbon and oxygen isotope data from HRDZ-carbonate cements in Paleocene Grebe Formation sands, together with data from flanking Paleocene and Eocene limestone samples (Table 4), are plotted on Fig. 12a. With the exception of one sample which was taken from near a fault intersection in Skua 3 (see Fig. 12b), the data set shows a broad correlative trend. The range in  $\delta^{13}\text{C}$  is a consequence of mixing between two carbon sources, one being organically derived with  $\delta^{13}\text{C} \sim -25\text{\textperthousand}$  (and representing oxidation of migrating hydrocarbons within the HRDZs) and the other with  $\delta^{13}\text{C} \sim 0\text{\textperthousand}$ , representing syn-depositional or early diagenetic carbonate precipitated from marine connate waters.

The  $\delta^{18}\text{O}$  composition of a mineral is a function of both the temperature at which it is precipitated and the  $\delta^{18}\text{O}$  of the parental water. Some of the scatter in the data set could be due to most samples analysed being comprised of mixed carbonate phases which could have formed at different times and temperatures, and possibly from different pore waters. Broad correlation of the  $\delta^{13}\text{C}$  data with  $\delta^{18}\text{O}$  data could indicate a temperature effect, whereby the later cements of the HRDZs precipitated from waters of similar  $\delta^{18}\text{O}$  as those which were parental to the earlier carbonate cements. Alternatively, or in addition to the temperature effect, the introduction of leaking hydrocarbons to the Grebe Formation sands was also accompanied by the introduction of a new pore water of different  $\delta^{18}\text{O}$  that mixed with the preexisting connate water.

Both scenarios are feasible, since formation of the HRDZs has been shown to have been associated with both elevated temperatures and an aqueous fluid flow

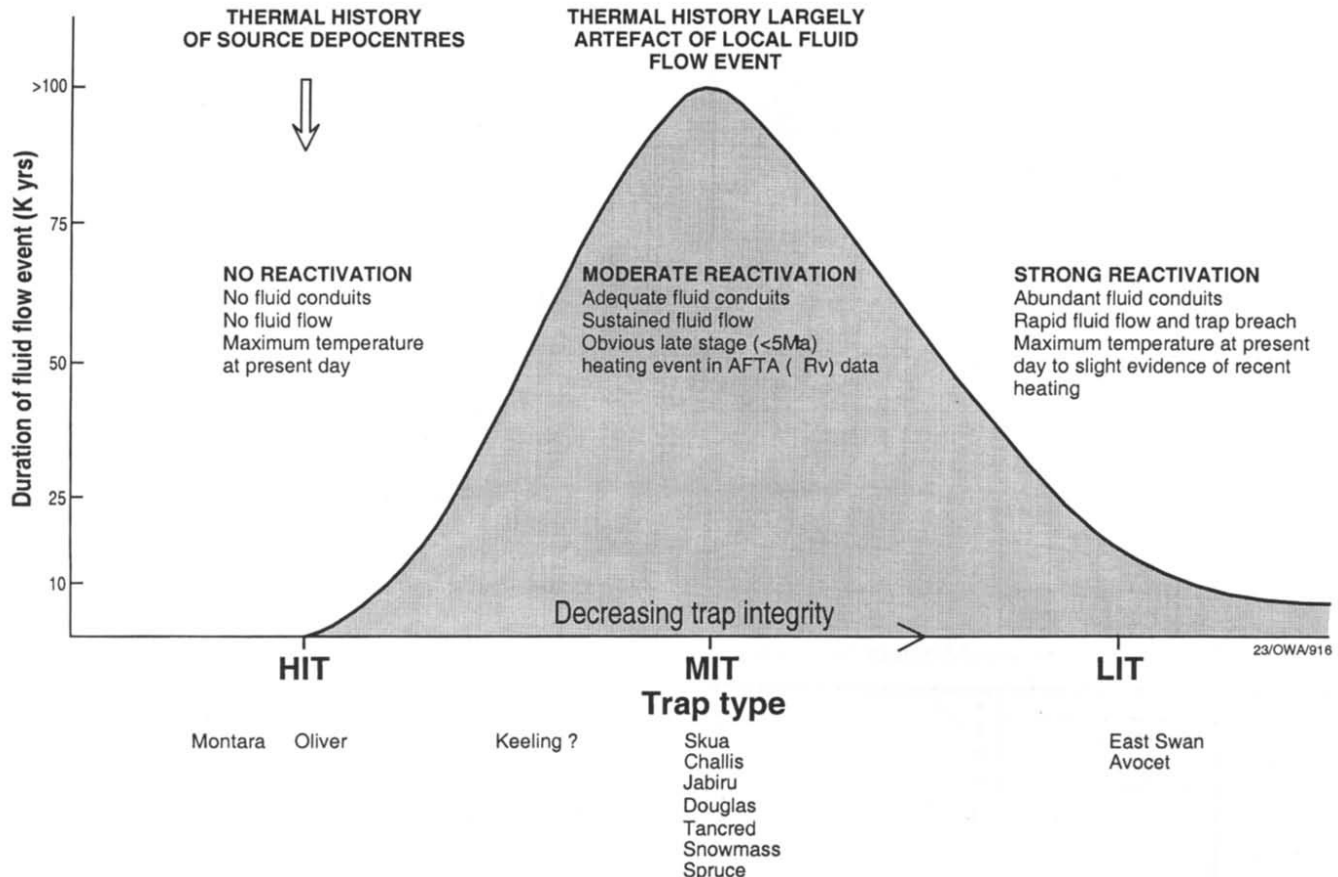


Fig. 11. Schematic representation of the nature and effects of the latest Miocene/Early Pliocene fluid flow event in the Timor Sea.

event associated with the migration of high salinity brines from (?) Siluro-Ordovician evaporites.

### 5.3.2. Strontium isotope data

In order to further characterise the fluid sources that may have been involved, some preliminary  $^{87}\text{Sr}/^{86}\text{Sr}$  analyses of calcite separates from three Paleocene/Eocene limestones and seven Grebe Formation (HRDZ-cemented) sands were made (Table 4). These data are plotted against the respective  $\delta^{13}\text{C}$  and  $\delta^{18}\text{O}$  analyses in Fig. 12c and d. There appears to be good correlation of both  $\delta^{13}\text{C}$  and  $\delta^{18}\text{O}$  with  $^{87}\text{Sr}/^{86}\text{Sr}$ .

Correlations between isotope ratios such as those seen in these figures are most easily interpreted in terms of two component mixing, whereby one end member has higher  $\delta^{13}\text{C}$  and  $\delta^{18}\text{O}$  and lower  $^{87}\text{Sr}/^{86}\text{Sr}$  than the other. The three isotope ratios for the three limestone samples are close to those expected for syn-depositional and early diagenetic carbonate precipitated from waters of marine origin and of Paleocene/Eocene age. This is regarded as one end member source of carbon, oxygen and strontium. The other end member is characterised by having lower  $\delta^{13}\text{C}$  and  $\delta^{18}\text{O}$  and, from the trends displayed in Fig. 12c and d, higher  $^{87}\text{Sr}/^{86}\text{Sr}$  and similar to the range of  $^{87}\text{Sr}/^{86}\text{Sr}$  ratios found for Lower Palaeozoic evaporites in Australia (unpublished CSIRO data).

The sample from Skua-3, which was taken from near a fault, appears to be anomalous with respect to the main trend of  $^{87}\text{Sr}/^{86}\text{Sr}$  versus  $\delta^{13}\text{C}$ , with  $\delta^{13}\text{C}$  and/or  $^{87}\text{Sr}/^{86}\text{Sr}$  being too high relative to the correlated trend of the remaining data (Fig. 12c). Similarly, with respect to the  $\delta^{13}\text{C}$  and  $\delta^{18}\text{O}$  correlation, this same sample is anomalous, with either  $\delta^{13}\text{C}$  and/or  $\delta^{18}\text{O}$  being too high (Fig. 12a and b). With respect to the  $^{87}\text{Sr}/^{86}\text{Sr}$  versus  $\delta^{18}\text{O}$  plot, this same sample appears to conform to the trend of the remaining samples, which implies that it is the  $\delta^{13}\text{C}$  value that is anomalously high and that this is a localised effect related to the sample's location near a fault.

Overall, the stable isotopic data support the proposal that aqueous fluids, sourced from Early Palaeozoic evaporites, passed through the Mesozoic and Tertiary sequences in the Mio-Pliocene.

## 6. Discussion of structural and fluid flow processes

Structural traps within Australia's Timor Sea can be classified by a tripartite classification scheme which has proved fundamental in developing an improved understanding both the structural integrity and the fluid flow and thermal histories, of traps in the region. This trap classification contains high integrity (HIT), moderate integrity (MIT) and low integrity (LIT) members.

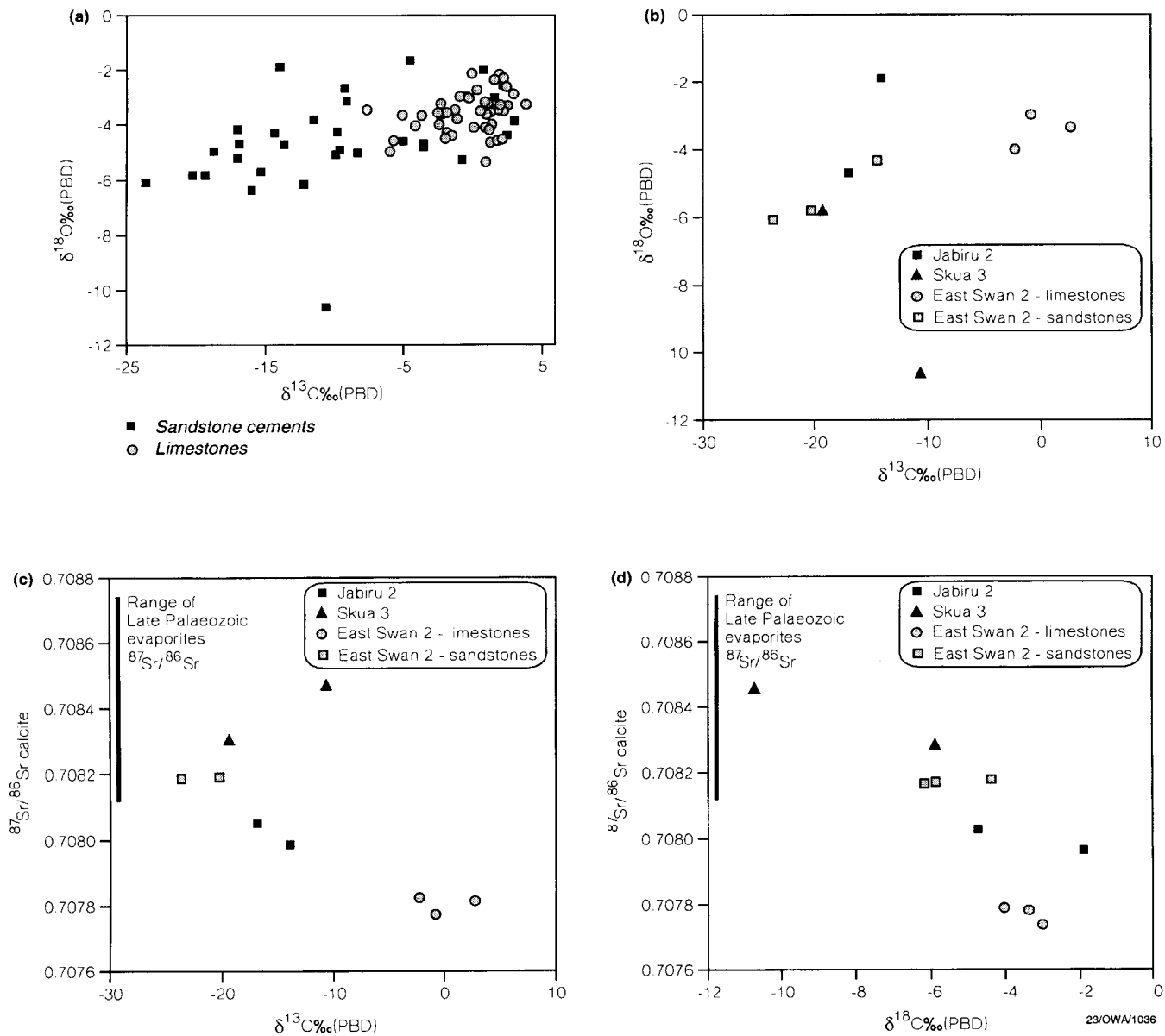


Fig. 12. Cross-plots showing the relationships between assorted variables for Tertiary samples from the Timor Sea. (a)  $\delta^{18}\text{O}$  versus  $\delta^{13}\text{C}$  for carbonate cemented sands (HRDZs) and flanking Tertiary limestones (all wells). (b)  $\delta^{18}\text{O}$  versus  $\delta^{13}\text{C}$  for carbonate cemented sands (HRDZs) and flanking Tertiary limestones for respective wells. (c)  $^{87}\text{Sr}/^{86}\text{Sr}$  versus  $\delta^{13}\text{C}$  for carbonate cemented sands (HRDZs) and flanking Tertiary limestones for respective wells. The range of strontium isotope compositions for Australian Palaeozoic evaporites is shown. (d)  $^{87}\text{Sr}/^{86}\text{Sr}$  versus  $\delta^{18}\text{O}$  for carbonate cemented sands (HRDZs) and flanking Tertiary limestones for respective wells. The range of strontium isotope compositions for Australian Palaeozoic evaporites is shown.

In the Late Miocene, the Timor Sea contained a large number of charged hydrocarbon traps, virtually all of which would now fall into the 'HIT' classification. At approximately 5–6 MaBP, the progressive oblique convergence of the Australian and Eurasian Plates began to induce significant, and rapid, fault reactivation in the Timor Sea. In particular, the rapid down-warping of the Timor Trough, effectively a proto-foreland basin, resulted in the localised bending of the Australian Plate down to the north-west. The bending induced significant flexural stress, resulting in the structural reactivation of

the Mesozoic and Palaeozoic rift faults, and the formation of shallow arrays of Mio-Pliocene extensional (and oblique extensional) faults. In particular, Mesozoic and Palaeozoic fault systems which were of large displacement tended to reactivate (dilatate) very strongly, resulting in the formation of a 'cone' of ENE-trending Mio-Pliocene fault 'damage', consisting of a broad array of large displacement, Mio-Pliocene faults. It is likely that faulting at this time took place via episodic, major earthquake activity (Muir-Wood, 1994; Sibson, 1994), in contrast to the relatively quiescent tectonic environment

Table 4

Carbon, oxygen and strontium isotope data (derived from cutting samples) from the Tertiary units in the Timor Sea, Australia

Well	Depth (m)	Lithology	Mineralogy <sup>a</sup>	$\delta^{13}\text{C} \text{‰}$ (PDB)	$\delta^{18}\text{O} \text{‰}$ (PDB)	$^{87}\text{Sr}/^{86}\text{Sr}$ (cal)
Skua-3	1160–70	Grebe sandstone	calcite	−10.73	−10.61	0.708471
Skua-3	1350–60	Grebe sandstone	7cal/26ank	−19.31	−5.8	0.708303
East Swan-2	1190–200	Grebe sandstone	13cal/11ank	−14.41	−4.31	0.7082
East Swan-2	1260–70	Grebe sandstone	23cal/12ank	−23.69	−6.07	0.708189
East Swan-2	1280–90	Grebe sandstone	25cal/11ank	−20.3	−5.8	0.708195
Jabiru-2	810	Grebe sandstone	cal	−17.01	−4.69	0.708053
Jabiru-2	850	Grebe sandstone	15cal/21ank	−14.07	−1.89	0.707989
East Swan-2	1000–10	Eocene carbonate	calcite	−2.32	−3.99	0.707826
East Swan-2	1330–40	Paleocene carbonate	86cal/4ank	−0.88	−2.98	0.707774
East Swan-2	1450–60	Paleocene carbonate	74cal/4ank	2.67	−3.34	0.707815

<sup>a</sup>cal means calcite and ank ankerite.<sup>87</sup>Sr/<sup>86</sup>Sr range of Early Palaeozoic Australian evaporites = 0.7081–0.7087 (CSIRO unpublished data).

which presently exists in the area, and which has existed since about 2.5–3 MaBP.

The processes of proto-foreland development and fault reactivation resulted in a major fluid flow event (Fig. 13). This fluid flow event involved the migration of hot (90–

120°C), saline (> 200,000 ppm) brines from deeply buried Palaeozoic evaporite sequences, probably from depths of 6–10 km, up major Mesozoic and Palaeozoic faults and through the Mesozoic and Tertiary sequences. The clear inference from this event is that fault reactivation in the

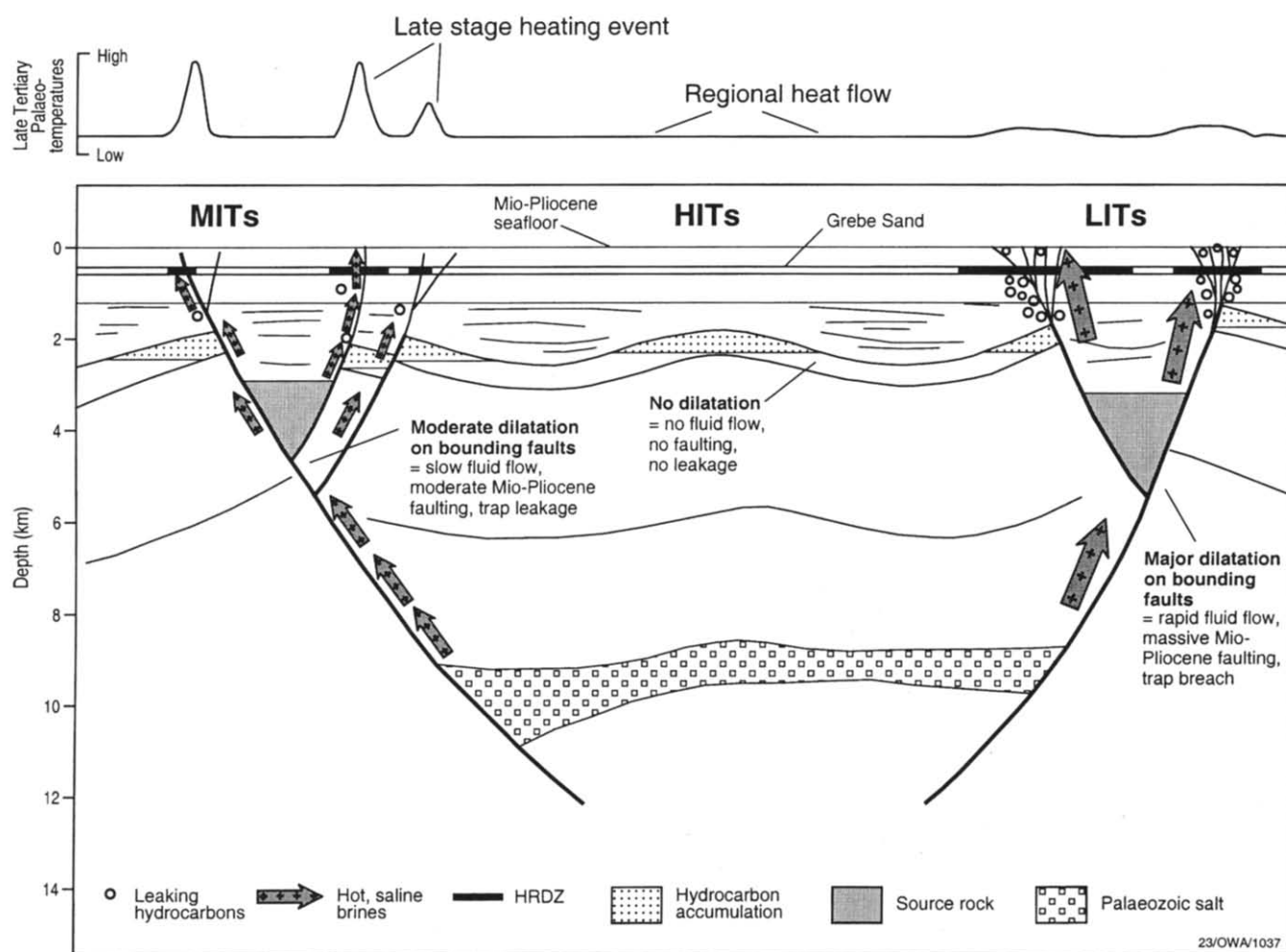


Fig. 13. Schematic representation showing the latest Miocene/Early Pliocene fluid flow event in the Timor Sea.

Timor Sea was driven from the 'bottom up', via the reactivation of deep, Jurassic and older-aged faults, and not from the 'top down', via shallow, Mio-Pliocene faulting. The small displacement Mio-Pliocene faults could never have provided adequate conduits from the Palaeozoic, through the Mesozoic reservoir intervals, to the surface. Where fault reactivation was sufficiently intense, the saline brines probably migrated through the reactivation fault arrays all the way to the palaeo-seafloor. The passage of these brines produced a localised, Late Tertiary (Mio-Pliocene), transient heating event which is evident in the fission track and fluid inclusion data in a number of wells. The evidence for the passage of the brines can only be seen in the residual hydrocarbon zones or the water zones of these wells, since the brines do not appear to have penetrated into the 'live' hydrocarbon-bearing zones.

The heating produced by the brines is most evident in MITs such as the Challis and Jabiru oil-fields. These underwent only moderate fault reactivation and, apparently as a consequence, leaked (i.e. the faults remained 'open') for a relatively extended period, certainly greater than 100,000 years, but less than 1,000,000 years. This allowed partial, but not complete, equilibration of the fission tracks in the apatite with the transient heat pulse.

In contrast, in traps which were reactivated very strongly (the LITs), the massive and rapidly developing Mio-Pliocene fault network facilitated very rapid trap breach and rapid passage of the brines. Modelling of the fission track data suggests that these traps experienced brine migration for only 10,000–100,000 years, which did not allow sufficient time for any thermal equilibration of the fission tracks with the passing fluids. This suggests that these traps breached catastrophically, probably via a series of closely spaced and massive earthquakes, with attendant fluid flow events.

High integrity traps did not experience late stage brine migration because of a lack of fault reactivation and attendant fluid flow pathways and, consequently, are now at their maximum temperatures. As such, the thermal histories of these traps probably most closely correspond to that undergone by the source rock kitchens in the Timor Sea.

In general, the fluid inclusion data, as evidenced best by Jabiru-1A and -2, have demonstrated that the brines appear most concentrated close to the fault-controlled zones of fluid flow (i.e. at Jabiru-2), then are progressively diluted away from the conduits (e.g. Jabiru-1A). This must take place via the progressive mixing (dilution) of the brines and connate waters within the Grebe aquifer, a proposal supported by the stable isotopic data. Nevertheless, the fact that minimal differences in thermal history (as determined via AFTA<sup>R</sup>) exist between Jabiru-2 and -1A, for example, indicates that the fluid flow did produce quite widespread thermal effects (either by con-

vection or diffusion), which extends beyond the localised conduit for fluid flow.

Where MITs and LITs were charged, hydrocarbon-related diagenetic zones or HRDZs formed contemporaneously with brine migration. Hydrocarbons, leaking from the Mesozoic reservoirs within the traps, migrated up the Mio-Pliocene faults which developed over the older rift faults. Upon entering the sands of a shallow (< 500 m deep) aquifer system, the Eocene Grebe Formation, the hydrocarbons were bacterially oxidised, which produced CO<sub>2</sub> for incorporation into massive carbonate cements (i.e. the HRDZs). The calcium, magnesium and sulphate required for the process were probably in large part provided via mixing with the immigrating saline brines, as it seems unlikely that the connate waters within the Grebe Formation would have had sufficient anions and cations to allow such massive carbonate cementation.

In the case of the MITs, the 'leaky fault segments', as delineated by the HRDZs, were very areally limited. Typically, the faults over partially breached, producing oil-fields such as Jabiru, Skua and Challis, only leaked for 200–1000 m along their length, and effectively constituted point sources of leakage (Fig. 14). In contrast, the faults over the breached LITs, such as Swift (Fig. 14) or East Swan, leaked in a continuous zone for several kilometres (3000–5000 m) along their length. HITs, such as Oliver-1, have not leaked at all. Paradoxically, as a result of their high integrity, coupled with increased thermal maturity of the source kitchens in the Neogene, these HITs have suffered gas-flushing within the last 3 million years, and are now subcommercial. With the charge history experienced in the Timor Sea, some leakiness in the traps is actually desirable, as it helps to preserve the hydrocarbon accumulations by reducing the risk of gas flushing.

Where moderate integrity and low integrity traps were not charged, the passage of the brines produced a thermal effect, though, due to the lack of hydrocarbons, no HRDZs were formed.

The above-mentioned observations on the length of the 'leaky' fault segments over various types of traps in the Timor Sea provides a key understanding for the development of exploration strategies in this area. For example, if remote sensing geochemical programs are being planned in this, or similar reactivated basins, and the principal exploration target is an MIT (i.e. a commercial oil-field), then the leaky segments over such a trap will effectively constitute point sources of seepage (usually less than 1000 m long). As such, the acquisition line spacings on such a program should be in the range 500–1500 m. If line spacings were to be significantly wider than this, for example 2000–6000 m, the only type of trap which might be identified consistently (provided it was still leaking) would probably be breached (i.e. LITs), clearly not a desirable outcome!

As such, a combination of detailed seismic mapping

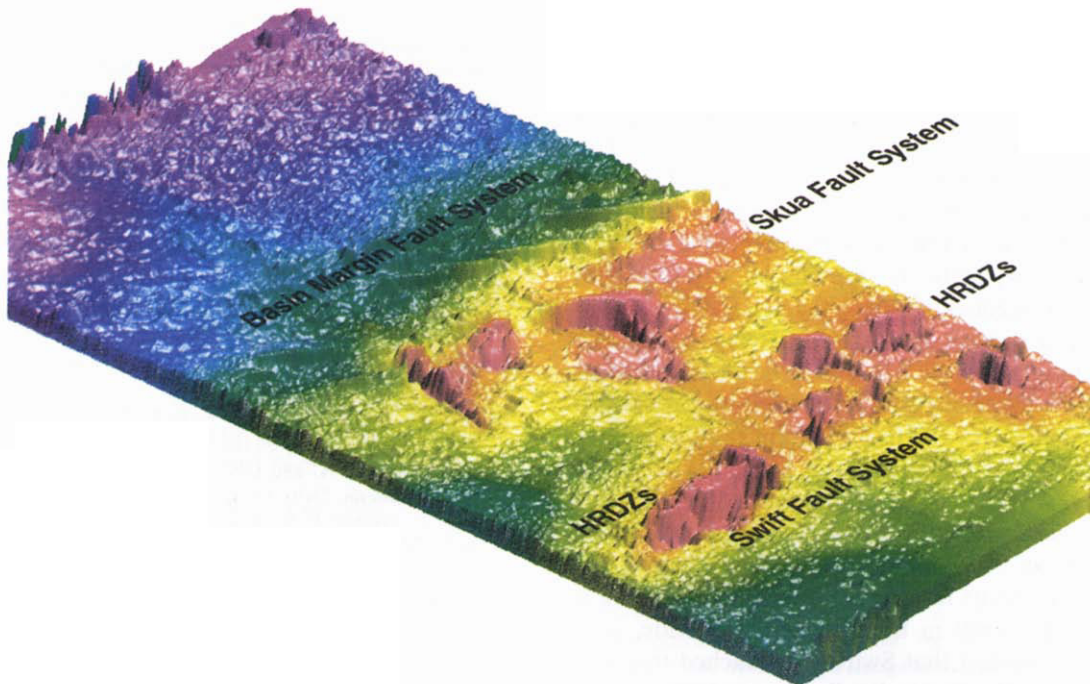


Fig. 14. Oblique view (from south-east) over the Skua and Swift accumulations in the Timor Sea at the Top Paleocene horizon. HRDZs, which define zones of carbonate cementation formed via mixing between hydrocarbons, saline brines and connate waters in the overlying Eocene section are purple and appear as en echelon, high velocity zones above the deeper Jurassic rift faults. The HRDZ associated with the breached Swift accumulation is over 4100 m long, much longer than the leaky fault segments over the producing Skua oil-field (typically 200–1000 m long).

(wherein the distribution of the HRDZs is mapped accurately and the Jurassic and Neogene fault geometries are characterised) and targeted remote sensing geochemical programs, probably represents the best way to reduce the exploration uncertainty in regard to trap integrity and charge in Australia's Timor Sea.

## 7. Addendum

### 7.1. Cross-disciplinary implications

Several of the observations made in this paper appear to be of direct relevance to the formation of low temperature (particularly lead-zinc) ore deposits. For example, many examples of mineralisation can be directly related to major tectonic events, and we have demonstrated that in the Timor Sea, continental collision and proto-foreland development have driven a major fluid flow event, which involved the migration of hot, saline brines from deeply buried evaporitic sequences. A common theme in recent publications on Pb-Zn mineralisation is that the mixing, at relatively low temperatures ( $< 130^{\circ}\text{C}$ ), of hydrocarbons, brines and connate waters is a key element in producing commercial grade ore deposits. Similarly, dolomitisation is a key cited factor in many mineral deposits. These are exactly the processes which are taking place within the Grebe Formation aquifer sands in the Mio-Pliocene in the Timor

Sea, during the formation of the HRDZs. In the Timor Sea, many of the factors necessary for mineralisation, such as brines, and hydrocarbons to act as a reductant for the metals, are present. Whether or not the brines in the Timor Sea are metal-rich, and have therefore produced mineralisation, remains to be determined, though undoubtedly the correct mix of geological processes is present.

Some of our observations could potentially assist in the understanding of older, low temperature mineral deposits. In particular, one advantage that this study has over observations made on ancient mineral deposits is that the processes that we have observed are geologically very recent ( $< \sim 5\text{--}6$  MaBP), and thus both the geology and the relevant processes are essentially 'pristine'. Moreover, high quality 2-D and 3-D seismic data are available in the Timor Sea, which allow detailed, well-constrained and unambiguous structural models to be developed, something lacking in old ore deposits.

Some of the key observations which may be of relevance are as follows:

- Zones of mixing of brines, hydrocarbons and connate waters (i.e. HRDZ formation) in the Timor Sea tend to take place along linear trends, something observed in mineral deposits, where mineralisation is often associated with 'lineaments'. However, in the Timor Sea, this linear distribution is often actually due to *en echelon* Mio-Pliocene faults (probably often Riedel

- shears) which have developed via the reactivation of the deeper Mesozoic rift faults (in response to continental collision and proto-foreland development). This geometry can be seen in Fig. 14, which shows an image-processed display (TWT time) for the Top Paleocene horizon over the Skua oil-field. The linear areas in purple are velocity anomalies (above the Paleocene) produced by HRDZ formation, which in turn have resulted in 'highs' in seismic two-way-time (but not depth). The zones of mixing (i.e. HRDZ formation) occur in two distinct trends, which relate to the two underpinning Mesozoic rift faults (the Skua and Swift faults). Note the strongly *en echelon* nature of the Miocene-Pliocene faults over the basin margin fault system to the north-west of the Skua Fault System. The size of the HRDZs varies along and between the different faults. Along the Skua fault trend, they typically range in length from 500–1500 m, with widths of up to 500 m. Along the Swift fault trend, the zone of mixing is approximately 4100 m long and 1000 m wide, consistent with the fact that Swift is a breached trap (see Fig. 14). Both the linear distribution and the sizes of the zones of mixing are similar to those often quoted for Pb-Zn deposits.
- In the Timor Sea, the relatively small HRDZs (200–1500 m long) which developed over the partially breached traps formed via mixing of hot (90–130 °C), saline (<200,000 ppm) brines, hydrocarbons and connate waters in an aquifer system for periods of between 100,000 and 1,000,000 years. In contrast, the data suggest that the mixing associated with the larger HRDZs (3000–5000 m long), which formed over the breached traps, probably took place for well under 100,000 years and perhaps for even less than 10,000 years. From a minerals perspective, this places definite limits on the time available to form ore deposits, and also would suggest that the potential to form richer deposits may be highest in the relatively smaller (200–1500 m long) zones of mixing, since brines flowed through these for much longer, through a more focussed conduit.

## Acknowledgements

This paper contributes to the Fill-Spill Project, a joint AGSO-CSIRO-Industry on charge history and trap integrity around the Australian continental margin and the Australian Geodynamics Cooperative Research Centre (AGCRC). The authors especially thank Lindell Emerton and Rex Bates for the cartographic efforts and the two anonymous reviewers whose comments substantially improved this paper. G. W. O'Brien publishes with the permission of the Director, AGSO.

## References

- Abbott, M. J., & Chamalaun, F. H. (1981). Geochronology of some Banda Arc volcanics. In *The geology and tectonics of eastern Indonesia* (pp. 253–268). Geological Research and Development Centre Special Publication.
- Aharon, P., Roberts, H. H., Sassen, R., Wheeler, C., & Feng, J. (1989). An isotope study of cold vents deposits from the continental slope, Gulf of Mexico: progress report. *Abstracts with Programs Geological Society of America*, 21(6), 273.
- Aharon, P., Roberts, H. H., Sassen, R., & Larkin, J. (1990). Stable isotopes and petrology of chimneys and calcareous fauna from hydrocarbon vents on the Gulf of Mexico slope. *Abstracts with Programs Geological Society of America*, 22(7), 208.
- Aharon, P., Gruber, E. R., & Roberts, H. H. (1991). Detection of hydrocarbon venting on the Gulf of Mexico sea floor from determinations of dissolved inorganic carbon and  $\delta^{13}\text{C}$  of the water column overlying seeps. *Transactions Gulf Coast Association of Geological Societies*, 41, 2–9.
- Aharon, P., Gruber, E. R., & Roberts, H. H. (1991). Detection of hydrocarbon venting on the Gulf of Mexico sea floor from determinations of  $\delta^{13}\text{C}$  and DIC of the water column overlying seeps. *AAPG Bulletin*, 75(9), 1514.
- Aharon, P., Gruber, E. R., & Roberts, H. H. (1992). Dissolved carbon and  $\delta^{13}\text{C}$  anomalies in the water column caused by hydrocarbon seeps on the northwestern Gulf of Mexico slope. *Geo Marine Letters*, 12(1), 33–40.
- Aharon, P., Roberts, H. H., & Snelling, R. (1992). Submarine venting of brines in the deep Gulf of Mexico: observations and geochemistry. *Geology*, 20(6), 483–486.
- Anderson, L. C., Aharon, P., & Sen Gupta, B. K. (1992). Methanotrophic gastropods from a bathyal hydrocarbon seep, Gulf of Mexico. *Abstracts with Programs Geological Society of America*, 24(7), 312.
- Baxter, K., Cooper, G. T., O'Brien, G. W., Hill, K. C., & Sturrock, S. (1997). Flexural isostatic modelling as a constraint on basin evolution, the development of sediment systems and palaeo-heat flow: application to the Vulcan Subbasin, Timor Sea. *APPEA Journal*, 37, 137–153.
- Bray, R. J., Green, P. F., & Duddy, I. R. (1992). Thermal history reconstruction in sedimentary basins usingapatite fission track analysis and vitrinite reflectance: a case study from the east Midlands of England and the southern North Sea. In R. F. P. Hardman, *Exploration Britain: geological insights for the next decade* (Vol. 67, pp. 3–25). Geological Society Special Publication.
- Brooks, J. M., Wiesenburg, D. A., Roberts, H. H., Carney, R. S., MacDonald, I. R., Fisher, C. R., Guinasso, N. L. Jr., Sager, W. W., McDonald, S. J., Burke, R. A. Jr., Aharon, P., & Bright, T. J. (1990). Salt, seeps and symbiosis in the Gulf of Mexico. *Eos, Transactions of the American Geophysical Union*, 71(45), 1772–1773.
- Duddy, I. R., Green, P. F., Bray, R. J., & Hegarty, K. A. (1994). Recognition of the thermal effects of fluid flow in sedimentary basins. In J. Parnell, *Geofluids: origin, migration and evolution in sedimentary Basins* (Vol. 78, pp. 325–345). Geological Society Special Publication.
- Duddy, I. R., Green, P. F., Hegarty, K. A., Bray, R. J., & O'Brien, G. W. (1997). Dating and duration of hot fluid flow events determined using AFTA' (apatite fission track analysis) thermal history reconstruction: extended abstract. In J. Hendry, et al., *Geofluids II '97* (pp. 10–13).
- Eadington, P. J., & Hamilton, P. J. (1990). Fluid migration and thermal history of Tithonian sandstones, Lower Swan Formation, Octavius 1 borehole, Timor Sea. *Unpublished CSIRO Report*.
- Eadington, P. J., Lisk, M., & Hamilton, P. J. (1990). Fluid history analysis of samples from Augustus 1, Douglas-1, Challis-1 and Jabiru-1A, Timor Sea. *Unpublished CSIRO Report*.
- Genrich, J., Bock, Y., McCaffrey, R., Calais, E., Stevens, C., Rais, J., Subaraya, C., & Puntodewo, S. S. O. (1995). Kinematics of the eastern Indonesia Island Arc estimated by global positioning system measurements. *EOS, Transactions, American Geophysical Union*, 75, 162.

- Geotechnical Services, 1996. Sediment investigations, Timor Sea, AC95-2, Geotechnical Services Pty. Ltd., Perth (34 pp.). *Unpublished*.
- Geotrack, 1987. Apatite fission track analysis of samples from Challis-1 and Jabiru-1, Timor Sea, Australia. *Geotrack Report No. 71*.
- Geotrack, 1988. Apatite fission track analysis of samples from Oliver-1, Timor Sea. *Geotrack Report No. 110*.
- Geotrack, 1997. Thermal history reconstruction using apatite fission track analysis and vitrinite reflectance. *Geotrack Report No. 577*.
- Gleadow, A. J. W., & Duddy, I. R. (1981). A natural long-term track annealing experiment for apatite. *Nuclear Tracks*, 5, 169–174.
- Gleadow, A. J. W., Duddy, I. R., & Lovering, J. F. (1983). Fission track analysis: a new tool for the evaluation of thermal histories and hydrocarbon potential. *APEA Journal*, 23, 93–102.
- Gleadow, A. J. W., Duddy, I. R., Green, P. F., & Lovering, J. F. (1986). Confined fission track lengths in apatite: a diagnostic tool for thermal history analysis. *Contributions to Mineralogy and Petrology*, 94, 405–415.
- Green, P. F., Duddy, I. R., Gleadow, A. J. W., & Lovering, J. F. (1989a). Apatite fission track analysis as a paleotemperature indicator for hydrocarbon exploration. In N. D. Naeser, & T. McCulloch, *Thermal history of sedimentary basins: methods and case histories* (pp. 181–195). New York: Springer-Verlag.
- Green, P. F., Duddy, I. R., Laslett, G. M., Hegarty, K. A., Gleadow, A. J. W., & Lovering, J. F. (1989). Thermal annealing of fission tracks in apatite: quantitative modelling techniques and extension to geological timescales. *Chemical Geology*, 79, 155–182.
- Graber, E. R., Aharon, P., & Roberts, H. H. (1990). Pore water carbonate chemistry from hydrocarbon vents on the Gulf of Mexico slope. *Abstracts with Programs Geological Society of America*, 22(7), 208.
- Harland, W. B., Armstrong, R. L., Cox, A. V., Craig, L. E., Smith, A. G., & Smith, D. G. (1990). *A geological timescale* (263 pp.). Cambridge: Cambridge University Press.
- Helby, R., Morgan, R., & Partridge, A. D. (1987). A palynological zonation of the Australian Mesozoic. In P. A. Jell, *Studies in Australian Mesozoic Palynology* (Vol. 4, pp. 1–94). Memoir: AAP.
- Hovland, M., Talbot, M. R. M., Qvale, H., Olaussen, S., & Aasberg, L. (1987). Methane-related carbonate cements in pockmarks of the North Sea. *Journal of Sedimentary Petrology*, 57, 81–892.
- Hovland, M., Croker, P. F., & Martin, M. (1994). Fault associated seabed mounds (carbonate knolls?) off western Ireland and north-west Australia. *Marine and Petroleum Geology*, 11(2), 232–246.
- Laslett, G. M., Kendall, W. S., Gleadow, A. J. W., & Duddy, I. R. (1982). Bias in measurement of fission track length distributions. *Nuclear Tracks*, 6, 79–85.
- Laslett, G. M., Green, P. F., Duddy, I. R., & Gleadow, A. J. W. (1987). Thermal annealing of fission tracks in apatite. 2. A quantitative analysis. *Chemical Geology*, 65, 1–13.
- Lisk, M., Hamilton, P. J., & Eadington, P. J. (1992). Fluid history analysis of samples East Swan-2 borehole, Timor Sea. *Unpublished CSIRO Report*.
- Lisk, M., O'Brien, G. W., & Brinca, M. P. (1997). Gas displacement and structural tilting: important controls on oil and gas distribution in the Timor Sea. *APPEA Journal*, 37, 259–271.
- McCaffrey, R. (1988). Active tectonics of the eastern Sunda and Banda arcs. *Journal of Geophysical Research*, 93(B12), 15163–15182.
- Muir-Wood, R. M. (1994). Earthquakes, strain-cycling and the mobilization of fluids. In J. Parnell, *Geofluids: origin, migration and evolution of fluids in sedimentary basins* (Vol. 78, pp. 85–98). *Geological Society Special Publication*.
- O'Brien, G. W. (1993). Some ideas on the rifting history of the Timor Sea from the integration of deep crustal seismic and other data. *PESA Journal*, 21, 95–113.
- O'Brien, G. W., & Woods, E. P. (1994). Vulcan subbasin, Timor Sea: clues to the structural reactivation and migration history from the recognition of hydrocarbon seepage indicators. *AGSO Research Newsletter*, 21, 8–11.
- O'Brien, G. W., & Woods, E. P. (1995a). Mapping hydrocarbon migration pathways via the integration of geophysical and geochemical data: Vulcan Subbasin, Timor Sea, north-western Australia. In *AAPG Annual Convention, Houston, March 5–9, 1995*.
- O'Brien, G. W., & Woods, E. P. (1995). Hydrocarbon-related diagenetic zones (HRDZs) in the Vulcan Subbasin, Timor Sea: recognition and exploration implications. *APEA Journal*, 35, 220–252.
- O'Brien, G. W., Etheridge, M. A., Wilcox, J. B., Morse, M., Symonds, P., Norman, D., & Needham, D. J. (1993). The structural architecture of the Timor Sea, north-western Australia: implications for basin development and hydrocarbon exploration. *APEA Journal*, 33(1), 258–278.
- O'Brien, G. W., Higgins, R., Symonds, P., Quaife, P., Colwell, J., & Blevin, J. (1996). Basement control on the development of extensional systems in Australia's Timor Sea: an example of hybrid hard linked/soft linked faulting? *APPEA Journal*, 36, 161–201.
- O'Brien, G. W., Lisk, M., Duddy, I., Eadington, P. J., Cadman, S., & Fellows, M. (1996). Late Tertiary fluid migration in the Timor Sea: a key control on thermal and diagenetic histories. *APEA Journal*, 36, 399–427.
- O'Brien, G. W., Woods, E. P., Lisk, M., & Fellows, M. (1996c). Hydrocarbon-related diagenesis: the key to understanding trap integrity and hydrocarbon charge history in Australia's Timor Sea? In *AAPG Bulletin Abstract, San Diego Conference, May 1996*.
- O'Brien, G. W., Lisk, M., & Duddy, I. R. (1997). Fault reactivation as a primary control on trap breach and fluid migration histories: Timor Sea, north-western Australia. In J. Hendry, et al., *Geofluids II '97* (extended abstract, pp. 166–169).
- O'Brien, G. W., & Quaife, P. (1997). Something old, something new: the integration of old and new technologies to better evaluate trap integrity and reduce exploration risk in Australia's Timor Sea. In *Offshore Petroleum '97 Conference, Perth, WA, September 1997* (extended abstract).
- O'Brien, G. W., Quaife, P., & Messent, B. (1998a). A multidisciplinary evaluation of the key controls on trap integrity in Australia's Timor Sea using integrated remote sensing technologies. *American Association of Petroleum Geologists Bulletin* (extended abstract).
- O'Brien, G. W., Quaife, P., Cowley, R., Morse, M., Wilson, D., Fellows, M., & Lisk, M. (1998b). Evaluating trap integrity in the Vulcan Subbasin, Timor Sea, Australia, using integrated remote sensing geochemical technologies. In P. G. Purcell, & R. R. Purcell, *Petroleum Exploration Society of Australia (PESA) Western Australian Basins Symposium* (Vol. 2, pp. 237–254).
- Pattillo, J., & Nicholls, P. J. (1990). A tectonostratigraphic framework for the Vulcan Graben, Timor Sea region. *APEA Journal*, 30(1), 27–51.
- Richard, P. D., Naylor, M. A., & Koopman, A. (1995). Experimental models of strike-slip tectonics. *Petroleum Geoscience*, 1, 71–80.
- Roberts, H. H., Sassen, R., & Aharon, P. (1987). Carbonates of the Louisiana continental slope. *Proceedings Offshore Technology Conference*, 19(2), 373–382.
- Roberts, H. H., Sassen, R., Carney, R., & Aharon, P. (1989).  $^{13}\text{C}$  depleted authigenic carbonate buildups from hydrocarbon seeps, Louisiana continental slope. *Transactions Gulf Coast Association of Geological Societies*, 39, 523–530.
- Roberts, H. H., Sassen, R., Carney, R., & Aharon, P. (1989). Carbonate buildups on the continental slope off central Louisiana. *Proceedings Offshore Technology Conference*, 21(1), 655–662.
- Roberts, H. H., Sassen, R., Carney, R., Aharon, P., & Portier, R. (1989). Reef-like carbonate buildups on the Louisiana continental slope. *Transactions Gulf Coast Association of Geological Societies*, 39, 587.
- Roberts, H. H., Aharon, P., Carney, R., Larkin, J., & Sassen, R. (1990). Sea floor responses to hydrocarbon seeps, Louisiana continental slope. *Geo Marine Letters*, 10(4), 232–243.

- Roberts, H. H., Aharon, P., & Mueller, J. (1991). Results from first direct observation and sampling of a Gulf of Mexico basin floor salt dome, Green Knoll. *AAPG Bulletin*, 75(9), 1536–1537.
- Sassen, R., Grayson, P., Cole, G., Roberts, H. H., & Aharon, P. (1991). Hydrocarbon seepage and salt dome related carbonate reservoir rocks of the US Gulf Coast. *AAPG Bulletin*, 75(9), 1537–1538.
- Sassen, R., Roberts, H. H., Aharon, P., Larkin, J., Chinn, E. W., & Carney, R. (1993). Chemosynthetic bacterial mats at cold hydrocarbon seeps, Gulf of Mexico continental slope. *Organic Geochemistry*, 20(1), 77–89.
- Sibson, R. H. (1994). Crustal stress, faulting and fluid flow. In J. Parnell, *Geofluids: origin, migration and evolution of fluids in sedimentary basins* (Vol. 78, pp. 69–84). Geological Society Special Publication.
- Ziaigos, J. P., & Blackwell, D. D. (1986). A model for the transient temperature geothermal systems. *Journal of Volcanology and Geothermal Research*, 27, 371–397.